Estimation of surface energy fluxes in the Arctic tundra using the remote sensing thermal-based Two-Source Energy Balance model

Jordi Cristóbal[1,2], Anupma Prakash[1], Martha C. Anderson[3], William P. Kustas[3], Eugénie S. Euskirchen[4], Douglas L. Kane[2]

5 [1]Geophysical Institute. University of Alaska Fairbanks, Fairbanks, Alaska, 99775, USA
[2]Institute of Northern Engineering. Water Environmental Research Center, University of Alaska Fairbanks, Fairbanks, Alaska, 99775, USA
[3]Hydrology and Remote Sensing Laboratory, United States Department of Agriculture, Agriculture Research Service, Beltsville, Maryland, 20705, USA
10 [4]Institute of Arctic Biology. University of Alaska Fairbanks, Fairbanks, Alaska, 99775, USA

Correspondence to: Jordi Cristóbal (j.cristobal@alaska.edu)

Abstract. The Arctic has become generally a warmer place over the past decades leading to earlier snow melt, permafrost degradation and changing plant communities. Increases in precipitation and local evaporation in the Arctic, known as the acceleration components of the hydrologic cycle, coupled with land cover changes, have resulted in significant changes in
15 the regional surface energy budget. Quantifying spatiotemporal trends in surface energy flux partitioning is a key to forecasting ecological responses to changing climate conditions in the Arctic. An extensive local evaluation of the two-source energy balance model (TSEB) - a remote sensing-based model using thermal infrared retrievals of land-surface temperature - was performed using tower measurements collected over different tundra types in Alaska in all sky conditions over the full growing season from 2008 to 2012. Based on comparisons with flux tower observations, refinements in the
20 original TSEB net radiation, soil heat flux and canopy transpiration parameterizations were identified for Arctic tundra. In particular, a revised method for estimating soil heat flux based on relationships with soil temperature was developed, resulting in significantly improved performance. These refinements result in mean turbulent flux errors generally less than 50 W·m^{-2} at half-hourly timesteps, similar to errors typically reported in surface energy balance modelling studies conducted in more temperate climatic regimes. The MODIS leaf area index (LAI) remote sensing product proved to be useful for
25 estimating energy fluxes in Arctic tundra in the absence of field data on local biomass amount. Model refinements found in this work at the local scale build toward a regional implementation of the TSEB model over Arctic tundra ecosystems, using thermal satellite remote sensing to assess response of surface fluxes to changing vegetation and climate conditions.

1 Introduction

Air temperatures in the Alaskan Arctic have shown a significant increase, especially in past decade (Serreze and Barry,
30 2011). Results from models forced with a range of climate scenarios from the Intergovernmental Panel on Climate Change (IPCC) indicate that by the mid-21st century the permafrost area in the Northern Hemisphere is likely to decrease by 37–

81% (IPCC, 2014). In general, the Arctic has become a warmer place, leading to an acceleration of the hydrologic cycle, earlier snow melt, and drier soils due to permafrost degradation (AMAP, 2012; Elmendorf et al., 2012; Rawlins et al., 2010; Sturm et al., 2001; Overduin and Kane, 2006). Furthermore, the hydrologic response of the Arctic land surface to changing climate is dynamically coupled to the region's surface energy balance (Vörösmarty et al., 2001), and the partitioning of

5   energy fluxes plays an important role in modulating the hydrologic cycle of Arctic basins (Rawlins et al., 2010).

Evapotranspiration (ET, in units of mass, kg s^{-1} m^{-2} or mm d^{-1}) or equivalently, latent heat flux (LE, in energy units, W·m^{-2}), is an important component of both the land surface hydrologic cycle and surface energy balance. As an example, Kane et al. (2004) reported water loss due to ET in the Imnavait Creek Basin in Alaska is about 74% of summer precipitation or 50% of annual precipitation, as estimated from water balance computations. Even though ET is a significant component of the

10   hydrologic cycle in Arctic regions, it is poorly quantified in Arctic basins, and the bulk estimates do not accurately account for spatial and temporal variability due to vegetation type and topography (Kane and Yang, 2004). In the Arctic, values of ET or LE are usually either derived from field estimates (Kane et al., 1990; Mendez et al., 1998) or calculated purely from empirical or quasi-physical models such as those described by Zhang et al. (2000) and Shutov et al. (2006) using meteorological station forcing data. However, due to remoteness, harsh winter conditions and the high costs of maintaining

15   ground-based measurement networks, the data currently collected are also both temporally and spatially sparse.

In Arctic tundra ecosystems, several factors have contributed to the vegetation change such as increased extent of severe fires, increased extent in deciduous vegetation or shrub encroachment in tundra ecosystems (Myers-Smith et al., 2011; Sturm et al., 2001), among others. Over at least the past three decades, Arctic ecosystems have shown evidence of "greening" (Xu et al., 2013; Bhatt et al., 2010), with about a 17% increase in peak vegetation greenness for the Arctic tundra biome (Jia et

20   al., 2003). Moreover, the forest-tundra transition zone is observed to be moving further north, tree heights are increasing, and shrubs are becoming denser and taller (ACIA, 2004; AMAP, 2012). These changes in vegetation will have an important impact on the surface energy balance, especially in areas where shrubs have made their appearance in former tundra vegetation. This increase in leaf area index (LAI), together with canopy height, and changes in the distribution of canopy elements, will augment the multiple scattering and absorption of radiation, likely resulting in a lower albedo (Beringer et al.,

25   2005), although more detailed observations and measurements, particularly for the beginning of the snow-free period and peak growing season are needed (Williamson et al., 2016). Also, according to Beringer et al. (2005), Bowen ratio increases from tundra to forested sites will result in an increasing dominance of sensible heat (H) as the primary energy source heating the atmosphere. In the case of a transition from tundra to tall shrub and then to forest, H would likely increase during the growing season from ~15% to nearly 30%, respectively. This will have an important impact in the tundra energy

30   partitioning, resulting in a positive feedback to the atmosphere that further warms the Arctic climate. However, the magnitude of changes in surface energy partitioning due to vegetation changes and resulting impact on local Arctic climate is still unclear and more research is needed to better understand these vegetation change-atmosphere dynamics (Eugster et al., 2000; Jung et al., 2010).

In the last two decades, surface energy balance methods have demonstrated their utility in modelling water availability using diagnostic retrievals of energy fluxes from *in situ* or remote sensing data, especially data acquired in the thermal infrared (TIR) region (Kalma et al., 2008). While remote sensing estimates of ET over the Arctic exist from global modelling systems (Mu et al., 2009; Zhang et al., 2010), these modelling systems typically do not compute the full energy balance. To estimate

5 energy fluxes at local scales, on the order of hundreds of meters, initiatives such as FLUXNET (http://fluxnet.ornl.gov/) provide eddy covariance flux measurements at discrete sites situated in different ecosystems across the U.S. and globally. Unfortunately, there are few measurements sites in the Arctic (Mu et al., 2009), making the existing instrument network insufficient to capture pertinent details of the changing Arctic climate and landscape (ACIA, 2004; AMAP, 2012; Serreze and Barry, 2011; Vörösmarty et al., 2001). Detailed process-based (prognostic) land-surface models can be also used to

10 estimate coupled water and energy fluxes over landscapes (Duursma and Medlyn, 2012; Ek et al., 2003; Falge et al., 2005; Haverd et al., 2013; Smith et al., 2001; Vinukollu et al., 2012, among others); however, they may neglect important processes that are not known a priori. For example, Hain et al. (2015) demonstrated the value of comparing prognostic and TIR-based diagnostic latent heat flux estimates over the continental U.S. to diagnose moisture sources and sinks that were not well-represented in the prognostic modelling system.

15 Given the critical need to better understand the water and energy balance over tundra ecosystems, and the role of changing climate and vegetation cover in driving these budgets, the aim of this work is to evaluate and refine a diagnostic TIR remote sensing-based model for estimating seasonal dynamics of surface energy fluxes (LE, H, net radiation (R_N) and soil heat flux (G)) as well as energy partitioning in the Arctic tundra growing season from 2008 to 2012. Specifically, a refined version of the Two-Source Energy Balance model (TSEB, Norman et al. (1995)) for Arctic tundra is evaluated with in situ forcing data

20 from three eddy covariance flux towers in all sky conditions, and remote sensing estimates of vegetation properties (LAI, NDVI (normalized difference vegetation index) and EVI (enhanced vegetation index)) from the Moderate Resolution Imaging Spectroradiometer (MODIS). Model refinements include a new G parameterization and new configurations to retrieve R_N (effective atmospheric emissivity), H and LE (two different Priestley-Taylor configurations). The TSEB serves as the land surface scheme in a regional Atmosphere-Land Exchange Inverse (ALEXI) modelling system (Anderson et al.,

25 2011), implemented operationally over North America as part of NOAA's GOES Evapotranspiration and Drought Information System. Although the TSEB has been demonstrated to work well over a range in vegetation and climate conditions at mid-latitudes (Anderson et al., 2007, 2011; Choi et al., 2009; Sánchez et al., 2009; Tang, et al., 2011; Timmermans et al., 2007, among others), it has not yet been examined for tundra ecosystems characteristic of high latitudes.

2 Two-Source Energy Balance model: an overview

30 Evapotranspiration (ET) can be estimated by surface energy balance models that partition the energy available at the land surface (R_N - G, where R_N is net radiation and G is the soil heat flux, both in W·m^{-2}) into turbulent fluxes of sensible and latent heating (H and LE, respectively, in W·m^{-2}):

3

$$LE + H = R_N - G, \tag{1}$$

where L is the latent heat of vaporization (J kg^{-1}) and E is ET (kg s^{-1} m^{-2} or mm s^{-1}).

The model used in this study is the series version of the Two-Source Energy Balance (TSEB) scheme originally proposed by Norman et al. (1995), which has been revised to improve shortwave and longwave radiation exchange within the soil–canopy system and the soil–canopy energy exchange (Kustas and Norman, 1999, 2000). A list of the TSEB inputs can be found in Table 1. TSEB has been successfully applied over rain fed and irrigated crops and grasslands in temperate and semi-arid climates (Anderson et al., 2012; Anderson et al., 2004; Cammalleri et al., 2012, 2010) but has not been previously applied over the Arctic tundra.

In the TSEB, directional surface radiometric temperature derived from satellite or a ground-based radiometer, $T_{RAD}(\theta)$ (K), is considered to be a composite of the soil and canopy temperatures, expressed as:

$$T_{RAD}(\theta) \approx [f_c(\theta)T_c^4 + (1 - f_c(\theta))T_s^4]^{1/4}, \tag{2}$$

where T_C is canopy temperature (K), T_S is soil temperature (K), and $f_C(\theta)$ is the fractional vegetation cover observed at the radiometer view angle θ. For a canopy with a spherical leaf angle distribution and LAI, $f_C(\theta)$ can be estimated as:

$$f_c(\theta) = 1 - exp\left(\frac{-0.5\Omega LAI}{cos\theta}\right), \tag{3}$$

where the factor Ω indicates the degree to which vegetation is clumped as in row crops or sparsely vegetated shrub land canopies (Kustas and Norman, 1999, 2000). The composite soil and canopy temperatures are used to compute the surface energy balance for the canopy and soil components of the combined land-surface system:

$$R_{NS} = H_S + LE_S + G, \tag{4}$$

$$R_{NC} = H_C + LE_C, \tag{5}$$

where R_{NS} is net radiation at the soil surface, R_{NC} is net radiation divergence in the vegetated canopy layer, H_C and H_S are canopy and soil sensible heat flux, respectively, LE_C is the canopy transpiration rate, LE_S is soil evaporation, and G is the soil heat flux. The net shortwave radiation is calculated from the measured incoming solar radiation and the surface albedo, while net longwave radiation is estimated from the observed air and land surface temperatures, using the Stefan-Boltzmann equation with atmospheric emissivity from the Brutsaert (1975) method.

By permitting the soil and vegetated canopy fluxes to interact with each other, Norman et al. (1995) derived expressions for H_S and H_C expressed as a function of temperature differences where:

$$H_S = \rho C_p \frac{T_S - T_{AC}}{r_S}, \tag{6}$$

and

$$H_C = \rho C_p \frac{T_C - T_{AC}}{r_X}, \tag{7}$$

with the total sensible heat flux H = H_C + H_S expressed as:

$$H = \rho C_p \frac{T_{AC} - T_A}{r_A}, \tag{8}$$

where ρ is air density (kg·m^{-3}), C_p is the specific heat of air (kJ·kg^{-1}·K^{-1}), T_{AC} is air temperature in the canopy air layer (K), T_A is the air temperature in the surface layer measured at some height above the canopy (K), r_X is the total boundary layer resistance of the complete canopy of leaves (s m^{-1}), r_S is the resistance to sensible heat exchange from the soil surface (s m^{-1}) and r_A is aerodynamic resistance (s m^{-1}) defined by:

$$R_A = \frac{[ln((z_U-d_O)/z_{OM})-\Psi_M][ln((z_T-d_O)/z_{OM})-\Psi_H]}{k^2 u}, \tag{9}$$

In Eq. (9) d_O is the displacement height, u is the wind speed measured at height z_U, k is von Karman's constant ($\approx$0.4), z_T is the height of the T_A measurement, Ψ_M and Ψ_H are the Monin–Obukhov stability functions for momentum and heat, respectively, and z_{OM} is the aerodynamic roughness length.

The original resistance formulations are described in more detail in Norman et al. (1995) with revisions described in Kustas and Norman (1999) and Kustas and Norman (2000). Weighting of the heat flux contributions from the canopy and soil components is performed indirectly by the partitioning of the R_N between soil and canopy and via the impact on resistance values from the fractional amount and type of canopy cover (see Kustas and Norman, 1999).

For the latent heat flux from the canopy, the Priestley–Taylor formula is used to initially estimate a potential rate for LE_C:

$$LE_C = \alpha_{PTC} f_G \frac{\Delta}{\Delta+\gamma} R_{NC}, \tag{10}$$

where α_{PTC} is a variable quantity related to the Priestley–Taylor coefficient (Priestley and Taylor, 1972), but in this case defined exclusively for the canopy component, which was suggested for row crops by Tanner and Jury (1976) and normally set to an initial value of 1.2, Δ is the slope of the saturation vapour pressure versus temperature curve and γ is the psychrometric constant ($\sim$0.066 kPa °C^{-1}). f_G is the fraction of green vegetation that according to Guzinski et al. (2013) and Fisher et al., (2008) can be estimated through the normalized difference vegetation index (NDVI) and the enhanced vegetation index (EVI):

$$f_G = 1.2 \frac{EVI}{NDVI}, 0 \le f_G \le 1, \tag{11}$$

Under stress conditions, TSEB iteratively reduces α_{PTC} from its initial value. The TSEB model requires both a solution to the radiative temperature partitioning (Eq. 2) and the energy balance (Eqs. 6 and 7), with physically plausible model solutions for soil and vegetation temperatures and fluxes. Non-physical solutions, such as daytime condensation at the soil surface (i.e., $LE_S < 0$), can be obtained under conditions of moisture deficiency. This happens because LE_C is overestimated in these cases by the Priestley–Taylor parameterization, which describes potential transpiration. The higher LE_C leads to a cooler T_C and T_S must be accordingly larger to satisfy Eq. (7). This drives H_S higher, and the residual LE_S from Eq. (12) can become negative. If this condition is encountered by the TSEB scheme, αPTC is iteratively reduced until $LE_S \sim 0$ (expected for a dry soil/substrate surface). However there are instances where the vegetation is not transpiring at the potential rate but is not stressed due to its adaption to water and climate conditions (Agam et al., 2010) or the fact that not all the vegetation is green

or actively transpiring (Guzinski et al., 2013) (a thorough discussion of conditions that force a reduction in α_{PTC}, can be also found in Anderson et al. (2005) and Li et al. (2005)).

The latent heat flux from the soil surface is solved as a residual in the energy balance equation:

$$LE_S = R_{NS} - G - H_S, \tag{12}$$

5   with G estimated as a fraction of the net radiation at the soil surface (c_G):

$$G = c_G R_{NS}, \tag{13}$$

From midmorning to midday period the value of c_G can be typically assumed to be constant (Kustas and Daughtry, 1990;Santanello and Friedl, 2003). In this case, a typical value of $\sim$0.3 can be assumed for c_G based on experimental data from several sources (Daughtry et al., 1990). However, c_G value varies with soil type and moisture conditions as well as

10 time, due to the phase shift between G and R_{NS} over a diurnal cycle (Santanello and Friedl, 2003).

3 TSEB formulation refinements for Arctic tundra

3.1 Downwelling longwave radiation estimation: effective atmospheric emissivity for all sky conditions

The original TSEB formulation estimates the downwelling longwave radiation component of R_N using the effective atmospheric emissivity (ε) method described in Brutsaert (1975) for clear sky conditions:

15 $$\varepsilon = C(e/T_A)^{1/7}, \tag{14}$$

where e is the water pressure in millibars and T_A in K and C is 1.24 as in the original Brutsaert (1975) formulation. However, in this study TSEB is applied for all sky conditions, including clear sky, partially cloudy and overcast conditions. To estimate ε for all sky conditions Crawford and Duchon (1999) proposed a methodology that incorporated the Brutsaert (1975) clear-sky parameterization and the Deardorff (1978) cloudiness correction using a simple cloud modification

20 introducing a cloud fraction term (clf) according to the following equation:

$$\varepsilon = \{clf + (1 - clf)[C(e/T_A)^{1/7}]\}, \tag{15}$$

The clf is defined as:

$$clf = 1 - s, \tag{16}$$

where s is the ratio of the measured solar irradiance to the clear-sky irradiance. Shortwave clear-sky irradiance used in Eq.

25 (16) may be obtained through the methodology proposed by Pons and Ninyerola (2008), where incident clear-sky irradiance is calculated through a digital elevation model at a specific point during a particular day of the year taking into account the position of the Sun, the angles of incidence, the projected shadows, the atmospheric extinction and the distance from the Earth to the Sun.

For Arctic areas, Jin et al. (2006) suggested an improved formulation of C for clear sky conditions that can also be applied in

30 Eq. (15) for all sky conditions, defined as:

$$C = 0.0003(T_A - 273.16)^2 - 0.0079(T_A - 273.16) + 1.2983, \tag{17}$$

In order to evaluate if the Jin et al. (2006) method offered more accurate estimates of ε for Arctic conditions, this method was compared to Brutsaert (1975) formulation used in TSEB, in both cases for all sky conditions using Eq. (15).

3.2 Refinements in soil heat flux parameterization: c_G coefficient and definition of a new coefficient based on T_{RAD}

In the Arctic tundra the propagation of the thawing front in the soil active layer consumes a large proportion (around 18%) of the energy input from the positive net radiation (Boike et al., 2008a; Rouse, 1985). Moreover, the presence of permafrost in tundra areas may contribute to the large tundra soil heat flux by creating a strong thermal gradient between the ground surface and depth, offsetting the influence of the highly insulative moss cover which would otherwise have been expected to reduce soil heat flux (Myers-Smith et al., 2011; Sturm et al., 2001). Therefore, previous formulations of soil heat flux used in TSEB applications, mainly representative of cropped and sparse-vegetated areas in the U.S., need to be adjusted and validated for Arctic tundra.

Currently there are several methodologies that allow estimating soil heat flux from tenths of centimetres to meters in depth in the Arctic tundra by using modelling or instrumentation at several depths (Lynch et al., 1999; Ekici et al., 2015; Jiang et al., 2015; Romanovsky et al., 1997; Yao et al., 2011; Zhuang et al., 2001; Hinzman et al., 1998). However, in this study a simple approach based on the relationship between G and R_{NS} (Eq. (13)) was used to estimate the soil heat flux in the near-surface soil layer (around 10 cm depth). This approach has less complexity and requires less input data than the methods mentioned above and allows estimating G at regional scales.

In early TSEB implementation, a constant value of c_G value around 0.3 was used to estimate G for the midmorning to midday period (Eq. (13) based on findings by Kustas and Daughtry (1990) for U.S. study sites. . However, this assumption can result in significant errors if applied out of this time range. For diurnal hourly timescales, Kustas et al. (1998), developed a method to estimate c_G based on time differences with the local solar noon quantified by a non-dimensional time parameter. Although this approach does not consider the phase shift between G and R_{NS} over a diurnal cycle, a phase shift was included in the model proposed by Santanello and Friedl (2003) in the following form:

$$c_G = A \, cos[2\pi(t + S)/B],\tag{18}$$

where A represents the maximum value of c_G, B is chosen to minimize the deviation of c_G from Eq. (13), t is time in seconds relative to solar noon and S is the phase shift between G and R_{NS} in seconds. Values fitted for A, S and B were 0.31, 10 800 and 74 000, respectively.

Although c_G values for Arctic tundra were not found in the literature, several studies present (Beringer et al., 2005; Eugster et al., 2005; Boike et al., 2008b; Eaton et al., 2001; Eugster et al., 2000; Kodama et al., 2007; Langer et al., 2011; Soegaard et al., 2001; Westermann et al., 2009; Mendez et al., 1998; Lund et al., 2014) the relationship between R_{NS} and G during the summer months in similar tundra areas. According to these studies, a mean value of 0.14, as a maximum value of c_G in Eq. (18), can be derived from different analyses of R_{NS} and G over the Arctic tundra.

An alternative parameterization for G suggested by Santanello and Friedl (2003) for several types of soils with crops, and by Jacobsen and Hansen (1999) for Arctic tundra that links the soil heat flux to the diurnal variations in surface radiometric temperature. This approach can also be applied for Arctic tundra as follows:

$$G = c_{TG}T_{RAD},$$ (19)

5 where c_{TG} is a coefficient that represents the relationship between the diurnal variation of T_{RAD} and G. For diurnal hourly timescales, c_{TG} can be also estimated using the phase shift proposed in Eq. (18); where in this case, S is the phase shift between G and T_{RAD} in seconds. This new approach avoids using R_{NS}, which is more difficult to define in tundra systems given the influence of the surface moss layer above the mineral soil. Moreover, A, S and B in Eq. (18) can be fitted by using direct measurements of T_{RAD} from thermal field sensors, commonly available on flux towers (pyrgeometer), or thermal data 10 from geostationary or polar satellites.

Thus, to evaluate soil heat flux for diurnal hourly timescales, the approaches of Kustas et al. (1998) and Santanello and Friedl (2003) were compared using the original c_G value of 0.30 and a new value for Arctic tundra of 0.14, both as maximum values of c_G in Eq. (18). A, B and S values for the new c_{TG} approach were fitted and tested using an extended evaluation dataset and then compared to these radiation-based methods (see section 4.2).

15 **3.3 Priestley-Taylor coefficient**

In the original TSEB formulation, the Priestley-Taylor approach for the canopy component of LE is used. In this case α_{PTC} is normally set to an initial value of 1.26 for the general conditions tested during the growing season in rangelands and croplands. For stressed canopies, TSEB internally modifies α_{PTC} to yield reasonable partitioning between LE_C and LE_S.

As with the c_G coefficient, specific α_{PTC} values for tundra were not found in the literature. Alternatively, measurements of 20 bulk (soil+canopy) for Arctic tundra systems are available (Beringer et al., 2005;Eaton et al., 2001;Eugster et al., 2005;Engstrom et al., 2002;Mendez et al., 1998;Lund et al., 2014) suggesting a mean value of around 0.92. This bulk value might suggest that α_{PTC} could also be lower for summer Alaska tundra conditions. For natural vegetation, Agam et al. (2010) also suggested that a lower α_{PTC} value might yield better results. Therefore, for modelling purposes two different values of α_{PTC} values, 0.92 and 1.26, were applied to evaluate which nominal α_{PTC} input to TSEB was more appropriate for Arctic 25 tundra.

4 Study area and data description

4.1 Study area

To refine and evaluate the TSEB model for Alaska's Arctic tundra summer conditions, three eddy covariance flux towers (referred to as Fen, Tussock and Heath; see Fig. 1) were selected. These are located across the Imnavait Watershed (~904 m

a.s.l.) with eddy covariance and associated meteorological data collection beginning in 2007 (Euskirchen et al., 2012; Kade et al., 2012). A brief description of instrumentation at the tower sites is provided in Table 2.

The Fen tower, located at the valley bottom in a wet sedge ecosystem, includes *Eriophorum angustifolium* and dwarf shrubs such as *Betula nana* and *Salix* spp and vegetation types around the tower are comprised of 52% wet sedge, and 47% tussock

5 tundra. The Tussock tower, located at the midslope in a moist acidic tussock tundra ecosystem, is dominated by the tussock-forming sedge *Eriophorum vaginatum*, *Sphagnum* spp., and dwarf shrubs such as *Betula nana* and *Salix* spp. In this case, vegetation types around the flux tower are 95% tussock tundra. The Heath tower sits atop a broad dry ridge at the top edge of the eastern watershed boundary in a heath tundra ecosystem dominated by dwarf shrubs and lichen. The vegetation here is 20% heath, but also included 72% tussock tundra, with the balance made of up of sedge meadow and bare soil. Further

10 detailed information about the study is provided in Euskirchen et al. (2012) and Trochim et al. (2015).

4.2 Model inputs, evaluation datasets, and metrics

4.2.1 Micrometeorological input data

Data incorporated in this study spanned from May to September 2008 to 2012. These included eddy covariance data for latent and sensible collected at 10 Hz and processed to 30-minute means (described below) as well as meteorological data

15 collected at 30-minute intervals (Table 1 and Table 2). These data, from under all sky conditions, were used to refine and evaluate the model performance (Table 1). This dataset was considered to be representative of the short Arctic tundra vegetative cycle from early growing to senescence as well as to capture inter- and intra-annual vegetation dynamics.

Meteorological input for TSEB include wind speed, air temperature, vapour pressure, atmospheric pressure, longwave incoming radiation and solar radiation, all of which were collected at the three measurement sites (see Table 1 and 2). The

20 surface radiometric temperature T_{RAD} inputs were obtained from the pyrgeometer sensor at the Tussock station and from infrared radiometer sensors at both Fen and Heath stations.

4.2.2 Remote sensing input data: vegetation properties

In addition, TSEB also requires estimates of LAI and the fraction of vegetation that is green to specify f_C in Eq. (2) and to estimate LE_C in Eq. (10). While, *in situ* measurements of LAI were not available at the tower sites for the length of this

25 study, the 500 m combined Terra/Aqua MODIS 4-day LAI product (MCD15A3H) was available for the study area. This product has been successfully applied in other applications of the TSEB (Guzinski et al., 2013) where sites are considered homogeneous over several kilometres, and serve here as a proxy for local observations. The fraction of vegetation that is green (f_G) in Eq. (10) was estimated using NDVI and EVI from MODIS imagery using the daily 250 m reflectance product (MOD09GQ), and using the blue band in the daily 500 m reflectance product 500 m (MOD09GA) to correct for residual

30 atmospheric effects, with negligible spatial artifacts. Because of MODIS time series contains occasional lower quality data, gaps from persistent clouds, cloud contamination, and other gaps (Gao et al., 2008), a program for analysing time series of

9

remote sensing imagery, TIMESAT (Jönsson and Eklundh, 2004) was used to produce temporally smoothed NDVI, EVI and LAI by selecting the best estimates through these products quality flags. Gao et al. (2008) found a good agreement with field measurements when smoothing MODIS LAI data using this distribution and several weights (w) based on the product quality flags (w = 1.0 for LAI retrievals from the radiative-transfer model (high quality) or for LAI retrieval that reaches

5   saturation, w = 0.25 for retrievals from an empirical model and w = 0.0 for all invalid and fill values). Beck et al. (2006) also reported that an asymmetric Gaussian distribution was appropriate for describing vegetation dynamics using NDVI at high latitudes and several weights (w) based on the product quality flags (highest quality/clear, mixed and cloudy were assigned weights of 1, 0.5 and 0, respectively). For NDVI, EVI and LAI time series smoothing, the weights and quality flags proposed by Beck et al. (2006) and Gao et al. (2008) were used.

10   Vegetation height, used to define roughness parameters d_O and z_{OM}, was assigned based on measurements made in the vicinity of the flux towers (Kade et al., 2012) and the clumping factor was set to 1 for all sites based on the knowledge that Arctic tundra has a variable moss layer with little bare ground. Variability regarding these inputs for the studied periods is shown in Table 1. Moreover, to ensure that only snow-free periods were analysed, Terra/Aqua MODIS snow cover products (MOD10A1 and MYD10A1) were used to screen days with snow cover at the beginning and end of the growing season.

15

4.2.3 Micrometeorological flux data for model evaluation

The eddy covariance data used in TSEB evaluation, including latent and sensible heat, were processed with EddyPro® (2004) software. Changes in mass flow caused by changes in air density (Webb et al., 1980), corrections for frequency attenuation of eddy covariance fluxes following Massman (2000) and Rannik (2001) and storage corrections for calm

20   periods (friction velocity (u*) was less than 0.1 m s^{-1} suggested by Rocha and Shaver (2011)) were accounted for. The automatic gain control (AGC) value (which represents optical impedance by precipitation) was computed for the IRGA and used as a QA/QC variable for both flux and radiation data, with 60 as the maximum threshold value (LI-COR 2004). Rejection angles of 10° were also used when the eddy covariance instruments were downwind of a tower to remove flow distortions. In addition, corrections for stationarity, lags, step-change, among others, were performed by the flux processing

25   software (for further information on micrometeorological data processing see Euskirchen et al. (2012) and http://aon.iab.uaf.edu/data_info). To select the best data available, the above criteria were used to flag the micrometeorological dataset, and no gap-filled data were used.

In addition, soil heat flux plate measurements were corrected to account for soil heat storage above the plate according to the calorimetric methodology proposed by Domingo et al. (2000) and Lund et al. (2014) using existing field measurements of

30   soil bulk density for each site (758 kg·m^{-3}, 989 kg·m^{-3} and 1038 kg·m^{-3} for Fen, Tussock and Heath flux stations, respectively), soil moisture from the water content reflectometer and thermocouple averaging soil temperature probes (TCAV) placed at two depths in the soil (see Table 2).

To evaluate the new c_{TG} approach, a total of 41068 half-hourly timesteps of T_{RAD} and G from 4 to 21 hours local solar time were selected (11593, 14454 and 15021 for Fen, Tussock and Heath flux stations, respectively). Coefficients *A*, *B* and *S* were

fitted using 60% of all available data (fitting subset) aggregated in 30 min timesteps for the whole summer period. The remaining 40% of the data were reserved for model testing (test subset) (see Table 4 for flux stations distribution). To evaluate the TSEB model, including G retrieve from Kustas et al. (1998) and Santanello and Friedl (2003) approaches, a total of 5178 half-hourly timesteps (1558, 1273 and 2347 for Fen, Tussock and Heath flux stations, respectively) was subset

5   from the previous selection by imposing three criteria: a) energy closure at the half-hourly timescale exceeded 70%, b) R_N was higher than 100 W·m^{-2} in order to ensure daylight conditions, and c) no precipitation present.

4.2.4 Evaluation metrics

For model evaluation, surface energy fluxes (R_N, LE, H and G) from the flux datasets (observed values) were compared to TSEB outputs (estimated values) using five metrics describing model errors and biases: the coefficient of determination (R^2)

10   was used to indicate the precision of the estimates in relation to observed surface energy fluxes; the root mean square error (RMSE) was used as a measure of accuracy to measure differences between values estimated by the TSEB model and values actually observed by the flux towers ; the mean bias error (MBE) was used to indicate cumulative offsets between measured and observed values; the mean absolute difference (MAD) was used to indicate the magnitude of the average absolute difference of observed and estimated values; and finally, the mean absolute percent difference (MAPD) was used to express

15   the magnitude of absolute difference between observed and estimated values relative to the observed mean value, from Eq. (20) to Eq. (24), respectively.

$$R^2 = \left(\frac{\sum_{i=1}^{n}(o_i-\bar{O})(e_i-\bar{E})}{\sqrt{\sum_{i=1}^{n}(o_i-\bar{O})^2}\sqrt{\sum_{i=1}^{n}(e_i-\bar{E})^2}} \right), \tag{20}$$

$$RMSE = \sqrt{\frac{\sum_{i=1}^{n}(e_i-o_i)^2}{n}}, \tag{21}$$

$$MBE = \frac{\sum_{i=1}^{n}(e_i-o_i)}{n}, \tag{22}$$

20    $$MAD = \frac{\sum_{i=1}^{n}|e_i-o_i|}{n}, \tag{23}$$

$$MAPD = \frac{100}{n}\left(\frac{\sum_{i=1}^{n}|e_i-o_i|}{\bar{O}}\right), \tag{24}$$

where e_i refers to the estimated value of the variable in question (R_N, H, LE or G), o_i is the observed value (*in situ* measurement provided by the flux station), n is the number of data points, and $\bar{O}$ and $\bar{E}$ are the average of the o_i and e_i values, respectively.

5 Results and discussion

5.1 Evaluation of soil heat flux model refinements for tundra

Both the Kustas et al., (1998; K98) and the Santanello and Friedl (2003; SF03) soil heat flux models used to estimate G at the study sites yielded high errors when a value of $c_G = 0.3$ was used, with MAPD ranging from 90% to 159%. In this case, the SF03 approach provided better results (Table 3). It is important to note that G is a relatively small term with a maximum value on the order of 50 $W·m^{-2}$. Both models generally overestimated G with a MBE from 3 $W·m^{-2}$ to 40 $W·m^{-2}$, with the SF03 model generating lower biases. Results improved when a c_G value of 0.14 was used with MAPD ranging from 48% to 76% and with lower RMSE values from 15 $W·m^{-2}$ to 21 $W·m^{-2}$ and MBE from -4 $W·m^{-2}$ to -14 $W·m^{-2}$. With the lower value of c_G, the K98 approach provided better results (Table 3).

Similar to the original c_G, c_{TG} can be also estimated using the Santanello and Friedl (2003) method in Eq. (18). Mean diurnal profiles in T_{RAD} and G, averaged over all tundra (see section 4.2 and Table 3) showed a phase shift between these variables (Fig. 2). The mean G value for the summer period peaked around 15:00 local solar time, with a phase shift around 4 hours after the maximum T_{RAD} at noon. Using T_{RAD} and G observations at half-hourly timesteps from the fitting subset, diurnal c_{TG} curves were derived for the growing season for each of the tower sites, showing reasonable agreement (Fig. 3). A fit to the mean curve yielded parameter values of S = -14 400 seconds, A = 1.55 and B = 160 000 s. As in the case of Santanello and Friedl (2003), a B variation of ± 15 000 s had no significant influence on the results. Statistical comparisons between observed fluxes from the test subset and simulations using the fitted parameters show good agreement and negligible bias (Table 4), with R^2, MAPD, RMSE and MBE values of 0.68, 37%, 6 $W·m^{-2}$ and 0 $W·m^{-2}$, respectively. In addition, the new model was also evaluated using the same flux subset used in Table 3 to assess the K98 and SF03 configurations, demonstrating improved performance with roughly half the MAPD than K98 and SF03 configurations (Table 4).

The performance of the G parameterization for Arctic tundra reported here is comparable or superior to previous studies reported in the literature using the Santanello and Friedl (2003) or Kustas et al. (1998) appoaches for other ecosystems. In shrub-grass dominated areas and boreal forest several studies (Anderson et al., 2008; Kustas et al., 1998; Li et al., 2008; Sánchez et al., 2009; Timmermans et al., 2007) reported MAPD and RMSE values ranging from 19% to 59% and from 15 $W·m^{-2}$ to 35 $W·m^{-2}$, respectively. Studies in corn and soybean crops (Anderson et al., 2005; Choi et al., 2009; Li et al., 2005; Santanello and Friedl, 2003) reported MAPD and RMSE values ranging from 19% to 34% and from 10 $W·m^{-2}$ to 41 $W·m^{-2}$, respectively.

5.2 Net radiation evaluation: effective atmospheric emissivity

Effective atmospheric emissivity estimated using the Brutsaert (1975) and Jin et al. (2006) methodologies yielded similar errors in simulated downwelling longwave radiation results, with a R^2 of 0.58 and a RMSE of 26 $W·m^{-2}$ and 27 $W·m^{-2}$, respectively. The C coefficient computed through Jin et al. (2006) yielded a value of 1.25 ±0.009, very close to Brutsaert (1975) C value of 1.24. This suggests that the simpler Brutsaert (1975) C coefficient can be used efficiently to model

effective atmospheric emissivity in all sky conditions when combined with Crawford and Duchon (1999) and Pons and Ninyerola (2008) methods for summer Arctic tundra.

Estimated R_N for all sky condition yielded strong agreement with observed values for all flux towers (see Fig. 4 and Table 5) with a mean R^2, MAPD, MAD, RMSE of 0.99, 7%, 18 W·m^{-2}, 23 W·m^{-2}, with a tendency to overestimate R_N with a MBE of 7 W·m^{-2}. In terms of RMSE and MAPD, all study sites behaved similarly (see Fig. 4). These results are in line with previous TSEB model applications for other cover types and clear sky conditions where a MAPD of around 5% was reported (Anderson et al., 2008; Li et al., 2005; Anderson et al., 2005; Kustas and Norman, 1999; Guzinski et al., 2013; Li et al., 2008; Anderson et al., 2000). This suggest that R_N estimation using this scheme can be applied regionally under summer all sky conditions in Arctic tundra when a source of solar radiation (METEOSAT or GOES, Cristóbal and Anderson (2013)), air temperature (Cristóbal et al., 2008) and T_{RAD} (MODIS Land Surface Temperature and emissivity product) are available.

5.3 Latent and sensible heat fluxes evaluation: α_{PTC} configuration for Arctic tundra

The average energy balance closure using half-hour periods for the evaluation dataset was 88% which is in agreement with the average closure of 90% for these flux stations, (Euskirchen et al., 2012). Lack of closure may be explained by instrument and methodological uncertainties, insufficient estimation of storage terms, unmeasured advective fluxes, landscape scale heterogeneity or instrument spatial representativeness, among others (Lund et al., 2014; Stoy et al., 2013; Foken et al., 2011; Foken, 2008; Wilson et al., 2002). More recently, there is evidence that non-orthogonal sonics underestimate vertical velocity causing under-measurement of H and LE on the order of 10% (Kochendorfer et al., 2012; Frank et al., 2013), although this is still being debated (Kochendorfer et al., 2013). While, currently, there is no uniform answer on how to deal with non-closure of the energy balance in eddy covariance datasets and methods for analysing the reasons for the lack of closure are still under discussion (Foken et al., 2011), in this study TSEB output is primarily compared with eddy covariance fluxes as observed, without closure corrections. However, to facilitate comparisons to numerous studies in the literature imposing energy conservation to eddy covariance data when evaluating surface energy balance models (Courault et al., 2005; Kalma et al., 2008), and given that strong evidence is presented in the literature that both H and LE are under-measured by the eddy covariance technique, additional comparisons with closed fluxes using the Bowen ratio (H_{BR} and LE_{BR}) approach suggested by Twin et al. (2000) and LE recalculated as the residual ($LE_{RES,}$ e.g., Li et al., 2008) are provided for completeness. Results with closed fluxes are presented to provide bounds on the range in probable model performance and to demonstrate the impact of closure corrections on model evaluation metrics.

LE and H estimated through both the new proposed soil heat flux methodology and the all sky R_N methodology scheme, yielded reasonable agreement with observed half-hourly unclosed turbulent fluxes, for both α_{PTC} parameterizations of 0.92 and 1.26 (see Tables 4 and 5, and Fig. 4), although $\alpha_{PTC} = 0.92$ yielded marginally lower errors for H and LE. Relative errors (MAPD) were 40 and 25% for LE and H, respectively, for all combined sites using $\alpha_{PTC} = 0.92$, and 45 and 27% using the

standard value of $\alpha_{PTC} = 1.26$, respectively. A slight improvement in H and LE estimates using $\alpha_{PTC} \sim 0.9$ also agrees with Agam et al. (2010) who also found better results with lower α_{PTC} for natural vegetation in water limited environments.

When energy balance closure is imposed, model performance is mainly improved for LE (up to 10% decrease in MAPD) in
5 part due to the fact that the measured turbulent fluxes are adjusted to achieve energy conservation as required by surface energy balance models. Indeed, the relatively small errors between modelled and measured R_N (Table 5) and relatively small and unbiased magnitude in modelled/measured G (Table 5 and Figure 4) suggests the unclosed turbulent fluxes contribute to the error statistics comparing Tables 5 and 6 with closed H and LE observed fluxes.

10 Nevertheless, since the mean RMSE for all fluxes compared to unclosed and closed turbulent fluxes and for all parameterizations and sites was around 50 W·m^{-2} (Table 5 and 6), which is commensurate with errors typically reported in other surface energy balance studies (Kalma et al., 2008), these results suggest that a generalized α_{PTC} value of 1.26 in global TSEB applications may adequately reproduce energy fluxes in Arctic tundra during the growing season, from leaf-out until senescence, while also capturing inter- and intra-annual dynamics. However, biases in regional applications may be reduced
15 by using a land cover class-dependent value of α_{PTC}.

Currently, there is limited research published on application of energy balance models to estimate energy fluxes for Arctic tundra. Mu et al. (2009) reported year-round errors from 20% to 40% in two Arctic tundra sites in Barrow (Alaska, USA) at daily periods based on a modified aerodynamic resistance–surface energy balance model where the required surface
20 conductance is estimated from remotely-sensed LAI based on Cleugh et al. (2007) formulation. TSEB results, however, were evaluated with half-hourly data in summer conditions and, although they cannot be directly compared with results in this previous study, they show similar errors. As in the case of R_N, LE and H results are also in line with previous works for other cover types using *in situ* data as input to TSEB (Anderson et al., 2000; Anderson et al., 2008; Li et al., 2005).

5.4 Seasonal dynamics of surface energy fluxes and energy partitioning

25 In general, monthly estimation of surface energy fluxes showed a good agreement with observations during the growing season. Because the model yielded similar results with both α_{PTC} parameterizations of 0.92 and 1.26, this section only shows the seasonal dynamics with α_{PTC} of 0.92. Because of the under-measurement issues with eddy covariance data and greater uncertainty and error associated with LE measurements (Wolf et al., 2008), seasonal dynamics of turbulent fluxes were compared with residual LE. Estimated R_N yielded a low MAPD around 6%, increasing up to 12% at the end of the growing
30 season (Table 7 and Fig. 5). The proposed new method to estimate G yielded better MAPD results from June to August which coincides with the peak of the growing season in July. A similar pattern was found for LE and H, where the best MAPD results occurred also in the middle of the growing season (June and July). MAPD for LE, H and G tended to be

14

higher in May and September; thus coinciding with earlier plant growth or the senesce periods, respectively. MODIS LAI product, used to estimate the fractional vegetation cover (Eq. 3) to partition soil and canopy temperatures, performed as a good proxy to capture inter- and intra-annual vegetation dynamics (Fig. 6). Mean seasonal MODIS LAI from May to September for all flux stations was 1.2 ± 0.5 $m^2 \cdot m^{-2}$. In previous studies close to the study area, Toolik Lake, and Imnaviat

5 Creek (Shaver and Chapin, 1991; Shippert et al., 1995; Williams et al., 2001; Williams et al., 2006) reported LAI field estimates ranging from 0.2 to 1.4 $m^2 \cdot m^{-2}$ for different tundra types around mid-July to mid-August, suggesting LAI overestimation from the MODIS product. Loranty et al. (2010) also reported LAI overestimation when using this product in similar tundra types, finding better agreement using a NDVI-LAI relationship (Shaver et al., 2007; Street et al., 2007), although the nonlinearity in the NDVI-LAI conversion is prone to averaging errors when scaled with remote sensing data

10 (Stoy et al., 2009). Despite MODIS LAI overestimation, it performed well for the Arctic tundra suggesting utility for regional applications, although LAI-NDVI methods might be considered for future applications.

f_G estimated through NDVI and EVI also captured inter- and intra-annual vegetation dynamics (Fig. 6), with a mean seasonal value from May to September for all flux stations of 0.82 ± 0.7. From May to August (from beginning and almost to the end of the growing period), f_G showed a good agreement with LAI dynamics. However, while f_G showed a steady increase at the

15 beginning of the growing season, it did not follow MODIS LAI dynamics in September. This caused the model to overestimate LE and underestimate H during this time period, degrading agreement with observed data. The underperformance of the f_G methods near the end of the growing season might be related to the presence of a variable moss layer, which can exert strong controls on understory water and heat fluxes in Arctic tundra ecosystems (Blok et al., 2011) and may have masked the actual vegetation dynamics (Fig. 6). Further research is needed to confirm this hypothesis. The

20 pattern of daily estimated surface energy fluxes also compared well to observed fluxes for all sky conditions. As an example, time series of modelled and measured surface energy fluxes are segmented in Fig. 7 for the Heath flux station, with each diurnal segment representing flux data averaged by hour over 5-day intervals from 2008 to 2012. Observed and estimated R_N exhibited an excellent agreement showing almost the same daily temporal pattern for the full growing season while LE, H and G yielded a good daily agreement being underestimated in May and September, especially in the case of LE.

25 In terms of observed ($_o$) and estimated ($_e$) mean season energy flux partitioning, LE_o/R_{No}, H_o/R_{No} and G_o/R_{No} yielded mean values of 0.55, 0.37 and 0.08, respectively; and LE_e/RN_e, H_e/R_{Ne} and G_e/R_{Ne} yielded mean values of 0.58, 0.34 and 0.08, respectively (Fig. 8). Observed and estimated Bowen ratio (β) yielded mean values of 0.60 and 0.67, respectively. In all cases, observed and estimated results are in line with previous studies for Arctic tundra (Lynch et al., 1999; Eugster et al., 2000). It is worth noting that the difference between observed and estimated values of LE/R_N, H/R_N partitions was only

30 around 3% and for G/R_N was almost negligible. From June to August, mean absolute difference values between observed and estimated values for LE/R_N, H/R_N were around 4%, increasing up to 15% in September due to model over and underestimation, while G/R_N difference was only less than 1%.

These results suggest that the model is able to reproduce accurately temporal trends of energy partition in concert with tundra vegetation dynamics in the growing vegetation peak from June to August and could be used to monitor changes in surface energy fluxes concurrently with vegetation dynamics.

6 Conclusions and future work

5   Parameterizations for R_N, G and α_{PTC} used in the two-source energy balance model (TSEB) were evaluated and refined for applications in different tundra types in Alaska over the full Arctic tundra growing season. Results showed that TSEB may adequately reproduce energy fluxes in Arctic tundra during the growing season, from leaf-out until senescence. The modified TSEB provided turbulent heat flux estimates with a mean RMSE value on the order of 50 $W \cdot m^{-2}$ in comparison with unclosed eddy covariance measurements of H and LE collected at three flux towers – commensurate with errors typically

10   reported in other surface energy balance studies. Moreover, as in many other studies using eddy covariance flux data for evaluating model performance, imposing energy balance closure yielded better agreement between measured and modelled turbulent fluxes. The all-sky R_N estimation scheme tested here yielded similar errors to those from other studies for only clear sky conditions. This demonstrates potential for regional scale applications when reliable sources of solar radiation, air temperature and T_{RAD} are available. A refined model for soil heat flux (G), based on the soil temperature-G relationship, was

15   evaluated from green-up to senescence using data for multiple years, and yielded errors half the magnitude of the standard TSEB formulation based on the relationship between R_{NS} and G. The TSEB α_{PTC} parameterization for estimating canopy transpiration (LEc) was tested using the standard TSEB value of 1.26 and a value of 0.92 suggested in the literature for Arctic tundra, and both parameterizations yield similar flux errors suggesting tundra-specific values of α_{PTC} are not needed. In the absence of in-situ measurements of LAI within the vicinity of the tower sites, the MODIS LAI product provided

20   reasonable inputs for localized model testing. The model was able to reproduce accurately temporal trends of energy partitioning in concert with tundra vegetation dynamics in the peak growing season. Moreover, it also has potential to monitor changes in surface energy fluxes in Arctic tundra due to changes in vegetation composition (e.g., shrub encroachment). This is particularly crucial in the Arctic where there is a sparse network of meteorological and flux observations. Further research is needed regarding the specific role of the moss layer in modifying remote sensing estimates

25   of green vegetation cover fraction and soil heat conduction within tundra ecosystems. Future work will incorporate the TSEB model refinements identified here for Arctic tundra into regional and global applications of the ALEXI surface energy balance modelling system. Model performance within a fully satellite-based remote sensing framework will be compared to the local evaluations reported here at these tundra flux sites. In addition, the diagnostic assessments of ET and surface energy fluxes will be compared with regional output from process-based

30   prognostic land-surface models to better understand the strengths and weaknesses of both types of modelling systems.

References

Agam, N., Kustas, W. P., Anderson, M. C., Norman, J. M., Colaizzi, P. D., Howell, T. A., Prueger, J. H., Meyers, T. P., and Wilson, T. B.: Application of the Priestley–Taylor Approach in a Two-Source Surface Energy Balance Model, J Hydrometeorol, 11, 185-198, doi:10.1175/2009jhm1124.1, 2010.

AMAP: Arctic Climate Issues 2011: Changes in Arctic Snow, Water, Ice and Permafrost. SWIPA 2011. Overview Report, Oslo, Norway, 96 pp., 2012.

Anderson, M. C., Norman, J. M., Meyers, T. P., and Diak, G. R.: An analytical model for estimating canopy transpiration and carbon assimilation fluxes based on canopy light-use efficiency, Agr Forest Meteorol, 101, 265-289, doi:10.1016/S0168-1923(99)00170-7, 2000.

Anderson, M. C., Norman, J. M., Mecikalski, J. R., Torn, R. D., Kustas, W. P., and Basara, J. B.: A multiscale remote sensing model for disaggregating regional fluxes to micrometeorological scales, J Hydrometeorol, 5, 343-363, 2004.

Anderson, M. C., Norman, J. M., Kustas, W. P., Li, F. Q., Prueger, J. H., and Mecikalski, J. R.: Effects of vegetation clumping on two-source model estimates of surface energy fluxes from an agricultural landscape during SMACEX, J Hydrometeorol, 6, 892-909, doi:10.1175/Jhm465.1, 2005.

Anderson, M. C., Kustas, W. P., and Norman, J. M.: Upscaling Flux Observations from Local to Continental Scales Using Thermal Remote Sensing, Agron J, 99, 240, doi:10.2134/agronj2005.0096S, 2007.

Anderson, M. C., Norman, J., Kustas, W., Houborg, R., Starks, P., and Agam, N.: A thermal-based remote sensing technique for routine mapping of land-surface carbon, water and energy fluxes from field to regional scales, Remote Sens Environ, 112, 4227-4241, doi:10.1016/j.rse.2008.07.009, 2008.

Anderson, M. C., Kustas, W. P., Norman, J. M., Hain, C. R., Mecikalski, J. R., Schultz, L., Gonzalez-Dugo, M. P., Cammalleri, C., d'Urso, G., Pimstein, A., and Gao, F.: Mapping daily evapotranspiration at field to continental scales using geostationary and polar orbiting satellite imagery, Hydrol Earth Syst Sc, 15, 223-239, doi:10.5194/hess-15-223-2011, 2011.

Anderson, M. C., Kustas, W. P., Alfieri, J. G., Gao, F., Hain, C., Prueger, J. H., Evett, S., Colaizzi, P., Howell, T., and Chávez, J. L.: Mapping daily evapotranspiration at Landsat spatial scales during the BEAREX'08 field campaign, Advances in Water Resources, 50, 162-177, doi:10.1016/j.advwatres.2012.06.005, 2012.

Beringer, J., Chapin, F. S., Thompson, C. C., and McGuire, A. D.: Surface energy exchanges along a tundra-forest transition and feedbacks to climate, Agr Forest Meteorol, 131, 143-161, doi:10.1016/j.agrformet.2005.05.006, 2005.

Beck, P. S. A., Atzberger, C., Hogda, K. A., Johansen, B., and Skidmore, A. K.: Improved monitoring of vegetation dynamics at very high latitudes: A new method using MODIS NDVI, Remote Sens Environ, 100, 321-334,
5 10.1016/j.rse.2005.10.021, 2006.

Bhatt, U. S., Walker, D. A., Raynolds, M. K., Comiso, J. C., Epstein, H. E., Jia, G. S., Gens, R., Pinzon, J. E., Tucker, C. J., Tweedie, C. E., and Webber, P. J.: Circumpolar Arctic Tundra Vegetation Change Is Linked to Sea Ice Decline, Earth Interact, 14, 1-20, Artn 8. doi:10.1175/2010ei315.1, 2010.

Blok, D., Heijmans, M. M. P. D., Schaepman-Strub, G., van Ruijven, J., Parmentier, F. J. W., Maximov, T. C., and
10 Berendse, F.: The Cooling Capacity of Mosses: Controls on Water and Energy Fluxes in a Siberian Tundra Site, Ecosystems, 14, 1055-1065, doi:10.1007/s10021-011-9463-5, 2011.

Boike, J., Hagedorn, B., and Roth, K.: Heat and Water Transfer Processes in Permafrost Affected Soils: A Review of Field and Modeling Based Studies for the Arctic and Antarctic, Plenary Paper, Proceedings of the 9th International Conference on Permafrost, June 29-July 3, 2008, University of Alaska, Fairbanks, USA, 2008a.

15 Boike, J., Wille, C., and Abnizova, A.: Climatology and summer energy and water balance of polygonal tundra in the Lena River Delta, Siberia, J Geophys Res-Biogeo, 113, Artn G03025, doi:10.1029/2007jg000540, 2008b.

Brutsaert, W.: On a derivable formula for long-wave radiation from clear skies, Water Resour Res, 11, 742-744, doi:10.1029/WR011i005p00742, 1975.

Cammalleri, C., Anderson, M. C., Ciraolo, G., D'Urso, G., Kustas, W. P., La Loggia, G., and Minacapilli, M.: The impact of
20 in-canopy wind profile formulations on heat flux estimation in an open orchard using the remote sensing-based two-source model, Hydrol Earth Syst Sc, 14, 2643-2659, doi:10.5194/hess-14-2643-2010, 2010.

Cammalleri, C., Anderson, M. C., Ciraolo, G., D'Urso, G., Kustas, W. P., La Loggia, G., and Minacapilli, M.: Applications of a remote sensing-based two-source energy balance algorithm for mapping surface fluxes without in situ air temperature observations, Remote Sens Environ, 124, 502-515, doi:10.1016/j.rse.2012.06.009, 2012.

25 Cammalleri, C., Anderson, M. C., Gao, F., Hain, C. R., and Kustas, W. P.: A data fusion approach for mapping daily evapotranspiration at field scale, Water Resour Res, 49, 4672-4686, doi:10.1002/wrcr.20349, 2013.

Cammalleri, C., Anderson, M. C., Gao, F., Hain, C. R., and Kustas, W. P.: Mapping daily evapotranspiration at field scales over rainfed and irrigated agricultural areas using remote sensing data fusion, Agr Forest Meteorol, 186, 1-11, doi:10.1016/j.agrformet.2013.11.001, 2014.

30 Choi, M., Kustas, W. P., Anderson, M. C., Allen, R. G., Li, F., and Kjaersgaard, J. H.: An intercomparison of three remote sensing-based surface energy balance algorithms over a corn and soybean production region (Iowa, U.S.) during SMACEX, Agr Forest Meteorol, 149, 2082-2097, doi:10.1016/j.agrformet.2009.07.002, 2009.

Cleugh, H. A., Leuning, R., Mu, Q. Z., and Running, S. W.: Regional evaporation estimates from flux tower and MODIS satellite data, Remote Sens Environ, 106, 285-304, doi:10.1016/j.rse.2006.07.007, 2007.

Courault, D., Seguin, B., and Olioso, A.: Review on estimation of evapotranspiration from remote sensing data: From empirical to numerical modeling approaches, Irrigation and Drainage Systems, 19, 223–249, 2005.

Crawford, T. M., and Duchon, C. E.: An improved parameterization for estimating effective atmospheric emissivity for use in calculating daytime downwelling longwave radiation, J Appl Meteorol, 38, 474-480, doi:10.1175/1520-0450;2, 1999.

5 Cristóbal, J., Ninyerola, M., and Pons, X.: Modeling air temperature through a combination of remote sensing and GIS data, Journal of Geophysical Research, 113, 1-13, doi:10.1029/2007jd009318, 2008.

Cristóbal, J., and Anderson, M. C.: Validation of a Meteosat Second Generation solar radiation dataset over the northeastern Iberian Peninsula, Hydrol Earth Syst Sc, 17, 163-175, doi:10.5194/hess-17-163-2013, 2013.

Daughtry, C. S. T., Kustas, W. P., Moran, M. S., Pinter, P. J., Jackson, R. D., Brown, P. W., Nichols, W. D., and Gay, L. W.:
10 Spectral Estimates of Net-Radiation and Soil Heat-Flux, Remote Sens Environ, 32, 111-124, doi:10.1016/0034-4257(90)90012-B, 1990.

Deardorff, J. W.: Efficient prediction of ground surface temperature and moisture, with inclusion of a layer of vegetation, Journal of Geophysical Research, 83, 1889, doi:10.1029/JC083iC04p01889, 1978.

Domingo, F., Villagarcia, L., Brenner, A. J., and Puigdefabregas, J.: Measuring and modelling the radiation balance of a
15 heterogeneous shrubland, Plant Cell Environ, 23, 27-38, doi:10.1046/j.1365-3040.2000.00532.x, 2000.

Eaton, A. K., Rouse, W. R., Lafleur, P. M., Marsh, P., and Blanken, P. D.: Surface energy balance of the western and central Canadian subarctic: Variations in the energy balance among five major terrain types, J Climate, 14, 3692-3703, doi:10.1175/1520-0442, 2001.

Duursma, R. A., and Medlyn, B. E.: MAESPA: a model to study interactions between water limitation, environmental
20 drivers and vegetation function at tree and stand levels, with an example application to CO2 × drought interactions, Geoscientific Model Development, 5, 919-940, 10.5194/gmd-5-919-2012, 2012.

Ek, M. B., Mitchell, K. E., Lin, Y., Rogers, E., Grunmann, P., Koren, V., Gayno, G., and Tarpley, J. D.: Implementation of Noah land surface model advances in the National Centers for Environmental Prediction operational mesoscale Eta model, J Geophys Res-Atmos, 108, n/a-n/a, Artn 885110.1029/2002jd003296, 2003.

25 Ekici, A., Chadburn, S., Chaudhary, N., Hajdu, L. H., Marmy, A., Peng, S., Boike, J., Burke, E., Friend, A. D., Hauck, C., Krinner, G., Langer, M., Miller, P. A., and Beer, C.: Site-level model intercomparison of high latitude and high altitude soil thermal dynamics in tundra and barren landscapes, Cryosphere, 9, 1343-1361, doi:10.5194/tc-9-1343-2015, 2015.

Elmendorf, S. C., Henry, G. H. R., Hollister, R. D., Bjork, R. G., Boulanger-Lapointe, N., Cooper, E. J., Cornelissen, J. H. C., Day, T. A., Dorrepaal, E., Elumeeva, T. G., Gill, M., Gould, W. A., Harte, J., Hik, D. S., Hofgaard, A., Johnson, D. R.,
30 Johnstone, J. F., Jonsdottir, I. S., Jorgenson, J. C., Klanderud, K., Klein, J. A., Koh, S., Kudo, G., Lara, M., Levesque, E., Magnusson, B., May, J. L., Mercado-Diaz, J. A., Michelsen, A., Molau, U., Myers-Smith, I. H., Oberbauer, S. F., Onipchenko, V. G., Rixen, C., Schmidt, N. M., Shaver, G. R., Spasojevic, M. J., Porhallsdottir, P. E., Tolvanen, A., Troxler, T., Tweedie, C. E., Villareal, S., Wahren, C. H., Walker, X., Webber, P. J., Welker, J. M., and Wipf, S.: Plot-scale evidence

of tundra vegetation change and links to recent summer warming, Nat Clim Change, 2, 453-457, doi:10.1038/Nclimate1465, 2012.

EddyPro® (Version 5) [Computer software]. 2014. Lincoln, NE. LI-COR, Inc; Infrastructure for Measurements of the European Carbon Cycle consortium.

5 Engstrom, R. N., Hope, A. S., Stow, D. A., Vourlitis, G. L., and Oechel, W. C.: Priestley-Taylor Alpha Coefficient: Variability and Relationship to Ndvi in Arctic Tundra Landscapes, J Am Water Resour As, 38, 1647-1659, doi:10.1111/j.1752-1688, 2002.

Eugster, W., Rouse, W. R., Pielke, R. A., McFadden, J. P., Baldocchi, D. D., Kittel, T. G. F., Chapin, F. S., Liston, G. E., Vidale, P. L., Vaganov, E., and Chambers, S.: Land-atmosphere energy exchange in Arctic tundra and boreal forest:

10 available data and feedbacks to climate, Global Change Biol, 6, 84-115, doi:10.1046/j.1365-2486, 2000.

Eugster, W., McFadden, J. P., and Chapin, F. S.: Differences in Surface Roughness, Energy, and CO2 Fluxes in Two Moist Tundra Vegetation Types, Kuparuk Watershed, Alaska, U.S.A., 2005.

Euskirchen, E. S., Bret-Harte, M. S., Scott, G. J., Edgar, C., and Shaver, G. R.: Seasonal patterns of carbon dioxide and water fluxes in three representative tundra ecosystems in northern Alaska, Ecosphere, 3, art4, 10.1890/es11-00202.1, 2012.

15 Falge, E., Reth, S., Bruggemann, N., Butterbach-Bahl, K., Goldberg, V., Oltchev, A., Schaaf, S., Spindler, G., Stiller, B., Queck, R., Kostner, B., and Bernhofer, C.: Comparison of surface energy exchange models with eddy flux data in forest and grassland ecosystems of Germany, Ecol Model, 188, 174-216, 10.1016/j.ecolmodel.2005.01.057, 2005.

Foken, T.: The energy balance closure problem: an overview, Ecol Appl, 18, 1351-1367, doi:10.1890/06-0922.1, 2008.

Foken, T., Aubinet, M., Finnigan, J. J., Leclerc, M. Y., Mauder, M., and U, K. T. P.: Results of a Panel Discussion About the

20 Energy Balance Closure Correction for Trace Gases, B Am Meteorol Soc, 92, Es13-Es18, doi:10.1175/2011BAMS3130.1, 2011.

Frank, J. M., Massman, W. J., and Ewers, B. E.: Underestimates of sensible heat flux due to vertical velocity measurement errors in non-orthogonal sonic anemometers, Agr Forest Meteorol, 171, 72-81, doi:10.1016/j.agrformet.2012.11.005, 2013.

Fisher, J. B., Tu, K. P., and Baldocchi, D. D.: Global estimates of the land-atmosphere water flux based on monthly AVHRR

25 and ISLSCP-II data, validated at 16 FLUXNET sites, Remote Sens Environ, 112, 901-919, doi:10.1016/j.rse.2007.06.025, 2008.

Gao, F., Morisette, J. T., Wolfe, R. E., Ederer, G., Pedelty, J., Masuoka, E., Myneni, R., Tan, B., and Nightingale, J.: An algorithm to produce temporally and spatially continuous MODIS-LAI time series, Ieee Geosci Remote S, 5, 60-64, 10.1109/Lgrs.2007.907971, 2008.

30 Guzinski, R., Anderson, M. C., Kustas, W. P., Nieto, H., and Sandholt, I.: Using a thermal-based two source energy balance model with time-differencing to estimate surface energy fluxes with day–night MODIS observations, Hydrol Earth Syst Sc, 17, 2809-2825, doi:10.5194/hess-17-2809-2013, 2013.

Hain, C. R., Crow, W. T., Anderson, M. C., and Yilmaz, M. T.: Diagnosing Neglected Soil Moisture Source-Sink Processes via a Thermal Infrared-Based Two-Source Energy Balance Model, J Hydrometeorol, 16, 1070-1086, 10.1175/Jhm-D-14-0017.1, 2015.

Haverd, V., Raupach, M. R., Briggs, P. R., Canadell, J. G., Isaac, P., Pickett-Heaps, C., Roxburgh, S. H., van Gorsel, E., Viscarra Rossel, R. A., and Wang, Z.: Multiple observation types reduce uncertainty in Australia's terrestrial carbon and water cycles, Biogeosciences, 10, 2011-2040, 10.5194/bg-10-2011-2013, 2013.

Hinzman, L. D., Goering, D. J., and Kane, D. L.: A distributed thermal model for calculating soil temperature profiles and depth of thaw in permafrost regions, J Geophys Res-Atmos, 103, 28975-28991, doi:10.1029/98jd01731, 1998.

IPCC, 2014: Climate Change 2014, Synthesis Report. Contribution of Working Groups I, II and III to the Fifth Assessment Report of the Intergovernmental Panel on Climate Change [Core Writing Team, R.K. Pachauri and L.A. Meyer (eds.)]. IPCC, Geneva, Switzerland, 2014

Jacobsen, A., and Hansen, B. U.: Estimation of the soil heat flux net radiation ratio based on spectral vegetation indexes in high-latitude Arctic areas, Int J Remote Sens, 20, 445-461, doi:10.1080/014311699213532, 1999.

Jia, G. J., Epstein, H. E., and Walker, D. A.: Greening of arctic Alaska, 1981–2001, Geophys Res Lett, 30, 2067, doi:10.1029/2003gl018268, 2003.

Jiang, Y. Y., Rocha, A. V., O'Donnell, J. A., Drysdale, J. A., Rastetter, E. B., Shaver, G. R., and Zhuang, Q. L.: Contrasting soil thermal responses to fire in Alaskan tundra and boreal forest, J Geophys Res-Earth, 120, 363-378, doi:10.1002/2014JF003180, 2015.

Jin, X., Barber, D., and Papakyriakou, T.: A new clear-sky downward longwave radiative flux parameterization for Arctic areas based on rawinsonde data, J Geophys Res-Atmos, 111, Artn D24104. doi:10.1029/2005jd007039, 2006.

Jung, M., Reichstein, M., Ciais, P., Seneviratne, S. I., Sheffield, J., Goulden, M. L., Bonan, G., Cescatti, A., Chen, J., de Jeu, R., Dolman, A. J., Eugster, W., Gerten, D., Gianelle, D., Gobron, N., Heinke, J., Kimball, J., Law, B. E., Montagnani, L., Mu, Q., Mueller, B., Oleson, K., Papale, D., Richardson, A. D., Roupsard, O., Running, S., Tomelleri, E., Viovy, N., Weber, U., Williams, C., Wood, E., Zaehle, S., and Zhang, K.: Recent decline in the global land evapotranspiration trend due to limited moisture supply, Nature, 467, 951-954, doi:10.1038/nature09396, 2010.

Jönsson, P., and Eklundh, L.: TIMESAT—a program for analyzing time-series of satellite sensor data, Comput Geosci-Uk, 30, 833-845, 10.1016/j.cageo.2004.05.006, 2004.

Kade, A., Bret-Harte, M. S., Euskirchen, E. S., Edgar, C., and Fulweber, R. A.: Upscaling of CO2 fluxes from heterogeneous tundra plant communities in Arctic Alaska, Journal of Geophysical Research, 117, doi:10.1029/2012jg002065, 2012.

Kalma, J. D., McVicar, T. R., and McCabe, M. F.: Estimating Land Surface Evaporation: A Review of Methods Using Remotely Sensed Surface Temperature Data, Surv Geophys, 29, 421-469, doi:10.1007/s10712-008-9037-z, 2008.

Kane, D. L., Gieck, R. E., and Hinzman, L. D.: Evapotranspiration from a Small Alaskan Arctic Watershed, Nordic Hydrology, 21, 253-272, 1990.

Kane, D. L., Gieck, R. E., Kitover, D. C., Hinzman, L. D., Mcnamara, J. P., and Yang, D.: Hydrologic Cycle on the North Slope of Alaska, 2004.

Kane, D. L., and Yang, D.: Overview for Water Balance Determinations for High Latitude Watersheds, 2004.

Kodama, Y., Sato, N., Yabuki, H., Ishii, Y., Nomura, M., and Ohata, T.: Wind direction dependency of water and energy

5   fluxes and synoptic conditions over a tundra near Tiksi, Siberia, Hydrol Process, 21, 2028-2037, doi:10.1002/hyp.6712, 2007.

Kongoli, C., Kustas, W. P., Anderson, M. C., Norman, J. M., Alfieri, J. G., Flerchinger, G. N., and Marks, D.: Evaluation of a Two-Source Snow–Vegetation Energy Balance Model for Estimating Surface Energy Fluxes in a Rangeland Ecosystem, J Hydrometeorol, 15, 143-158, doi:10.1175/jhm-d-12-0153.1, 2014.

10   Kustas, W. P., and Daughtry, C. S. T.: Estimation of the Soil Heat-Flux Net-Radiation Ratio from Spectral Data, Agr Forest Meteorol, 49, 205-223, doi:10.1016/0168-1923(90)90033-3, 1990.

Kustas, W. P., Zhan, X., and Schmugge, T. J.: Combining optical and microwave remote sensing for mapping energy fluxes in a semiarid watershed, Remote Sens Environ, 64, 116-131, doi:10.1016/S0034-4257(97)00176-4, 1998.

Kustas, W. P., and Norman, J. M.: Evaluation of soil and vegetation heat flux predictions using a simple two-source model

15   with radiometric temperatures for partial canopy cover, Agr Forest Meteorol, 94, 13-29, doi:10.1016/S0168-1923(99)00005-2, 1999.

Kustas, W. P., and Norman, J. M.: A two-source energy balance approach using directional radiometric temperature observations for sparse canopy covered surfaces, Agron J, 92, 847-854, 2000.

Kochendorfer, J., Meyers, T. P., Frank, J., Massman, W. J., and Heuer, M. W.: How Well Can We Measure the Vertical

20   Wind Speed? Implications for Fluxes of Energy and Mass, Bound-Lay Meteorol, 145, 383-398, doi:10.1007/s10546-012-9738-1, 2012.

Kochendorfer, J., Meyers, T. P., Frank, J. M., Massman, W. J., and Heuer, M. W.: Reply to the Comment by Mauder on "How Well Can We Measure the Vertical Wind Speed? Implications for Fluxes of Energy and Mass", Bound-Lay Meteorol, 147, 337-345, doi:10.1007/s10546-012-9792-8, 2012.

25   Langer, M., Westermann, S., Muster, S., Piel, K., and Boike, J.: The surface energy balance of a polygonal tundra site in northern Siberia - Part 1: Spring to fall, Cryosphere, 5, 151-171, doi:10.5194/tc-5-151-2011, 2011.

Li, F., Kustas, W. P., Anderson, M. C., Prueger, J. H., and Scott, R. L.: Effect of remote sensing spatial resolution on interpreting tower-based flux observations, Remote Sens Environ, 112, 337-349, doi:10.1016/j.rse.2006.11.032, 2008.

Li, F. Q., Kustas, W. P., Prueger, J. H., Neale, C. M. U., and Jackson, T. J.: Utility of remote sensing-based two-source

30   energy balance model under low- and high-vegetation cover conditions, J Hydrometeorol, 6, 878-891, doi:10.1175/Jhm464.1, 2005.

LI-COR Inc. LI-7500 CO_2/H_2O analyzer instruction manual. LI-COR, Lincoln, Nebraska, USA, 2004.

Loranty, M. M., Goetz, S. J., Rastetter, E. B., Rocha, A. V., Shaver, G. R., Humphreys, E. R., and Lafleur, P. M.: Scaling an Instantaneous Model of Tundra NEE to the Arctic Landscape, Ecosystems, 14, 76-93, doi:10.1007/s10021-010-9396-4, 2010.

Lund, M., Hansen, B. U., Pedersen, S. H., Stiegler, C., and Tamstorf, M. P.: Characteristics of summer-time energy exchange in a high Arctic tundra heath 2000-2010, Tellus B, 66, doi:10.3402/Tellusb.V66.21631, 2014.

Lynch, A. H., Chapin, F. S., Hinzman, L. D., Wu, W., Lilly, E., Vourlitis, G., and Kim, E.: Surface energy balance on the arctic tundra: Measurements and models, J Climate, 12, 2585-2606, doi:10.1175/1520-0442;2, 1999.

Massman, W. J.: A simple method for estimating frequency response corrections for eddy covariance systems, Agr Forest Meteorol, 104, 185-198, doi:10.1016/S0168-1923(00)00164-7, 2000.

Mendez, J., Hinzman, L. D., and Kane, D. L.: Evapotranspiration from a wetland complex on the Arctic coastal plain of Alaska, Nordic Hydrology, 29, 303-330, 1998.

Mu, Q. Z., Jones, L. A., Kimball, J. S., McDonald, K. C., and Running, S. W.: Satellite assessment of land surface evapotranspiration for the pan-Arctic domain, Water Resour Res, 45, Artn W09420 doi:10.1029/2008wr007189, 2009.

Myers-Smith, I. H., Forbes, B. C., Wilmking, M., Hallinger, M., Lantz, T., Blok, D., Tape, K. D., Macias-Fauria, M., Sass-Klaassen, U., Levesque, E., Boudreau, S., Ropars, P., Hermanutz, L., Trant, A., Collier, L. S., Weijers, S., Rozema, J., Rayback, S. A., Schmidt, N. M., Schaepman-Strub, G., Wipf, S., Rixen, C., Menard, C. B., Venn, S., Goetz, S., Andreu-Hayles, L., Elmendorf, S., Ravolainen, V., Welker, J., Grogan, P., Epstein, H. E., and Hik, D. S.: Shrub expansion in tundra ecosystems: dynamics, impacts and research priorities, Environmental Research Letters, 6, doi:10.1088/1748-9326/6/4/045509, 2011.

Norman, J. M., Kustas, W. P., and Humes, K. S.: Source Approach for Estimating Soil and Vegetation Energy Fluxes in Observations of Directional Radiometric Surface-Temperature, Agr Forest Meteorol, 77, 263-293, doi:10.1016/0168-1923(95)02265-Y, 1995.

Norman, J. M., Kustas, W. P., Prueger, J. H., and Diak, G. R.: Surface flux estimation using radiometric temperature: A dual-temperature-difference method to minimize measurement errors, Water Resour Res, 36, 2263, doi:10.1029/2000wr900033, 2000.

Overduin, P. P., and Kane, D. L.: Frost boils and soil ice content: Field observations, Permafrost Periglac, 17, 291-307, Doi 10.1002/Ppp.567, 2006.

Pons, X., and Ninyerola, M.: Mapping a topographic global solar radiation model implemented in a GIS and refined with ground data, Int J Climatol, 28, 1821-1834, doi:10.1002/Joc.1676, 2008.

Priestley, C. H. B., and Taylor, R. J.: On the assessment of surface heat flux and evaporation using large-scale parameters, Mon Weather Rev, 100, 81-92, 1972.

Rannik, Ü.: A comment on the paper by W.J. Massman 'A simple method for estimating frequency response corrections for eddy covariance systems', Agr Forest Meteorol, 107, 241-245, http://dx.doi.org/10.1016/S0168-1923(00)00236-7, 2001.

Rawlins, M. A., Steele, M., Holland, M. M., Adam, J. C., Cherry, J. E., Francis, J. A., Groisman, P. Y., Hinzman, L. D., Huntington, T. G., Kane, D. L., Kimball, J. S., Kwok, R., Lammers, R. B., Lee, C. M., Lettenmaier, D. P., McDonald, K. C., Podest, E., Pundsack, J. W., Rudels, B., Serreze, M. C., Shiklomanov, A., Skagseth, O., Troy, T. J., Vorosmarty, C. J., Wensnahan, M., Wood, E. F., Woodgate, R., Yang, D. Q., Zhang, K., and Zhang, T. J.: Analysis of the Arctic System for Freshwater Cycle Intensification: Observations and Expectations, J Climate, 23, 5715-5737, doi:10.1175/2010jcli3421.1, 2010.

Rocha, A. V., and Shaver, G. R.: Burn severity influences postfire CO2 exchange in arctic tundra, Ecol Appl, 21, 477-489, doi:10.1890/10-0255.1, 2011.

Romanovsky, V. E., Osterkamp, T. E., and Duxbury, N. S.: An evaluation of three numerical models used in simulations of the active layer and permafrost temperature regimes, Cold Reg Sci Technol, 26, 195-203, doi:10.1016/S0165-232x(97)00016-5, 1997.

Rouse, W. R.: Microclimate of Arctic Tree Line .2. Soil Microclimate of Tundra and Forest, Water Resour Res, 20, 67-73, doi:10.1029/Wr020i001p00067, 1984.

Sánchez, J. M., Caselles, V., Niclòs, R., Coll, C., and Kustas, W. P.: Estimating energy balance fluxes above a boreal forest from radiometric temperature observations, Agr Forest Meteorol, 149, 1037-1049, 10.1016/j.agrformet.2008.12.009, 2009.

Santanello, J. A., and Friedl, M. A.: Diurnal covariation in soil heat flux and net radiation, J Appl Meteorol, 42, 851-862, 2003.

Serreze, M. C., and Barry, R. G.: Processes and impacts of Arctic amplification: A research synthesis, Global Planet Change, 77, 85-96, doi:10.1016/j.gloplacha.2011.03.004, 2011.

Shaver, G. R., and Chapin, F. S.: Production - Biomass Relationships and Element Cycling in Contrasting Arctic Vegetation Types, Ecol Monogr, 61, 1-31, doi:10.2307/1942997, 1991.

Shaver, G. R., Street, L. E., Rastetter, E. B., Van Wijk, M. T., and Williams, M.: Functional convergence in regulation of net CO2flux in heterogeneous tundra landscapes in Alaska and Sweden, J Ecol, 95, 802-817, doi:10.1111/j.1365-2745.2007.01259.x, 2007.

Shippert, M. M., Walker, D. A., Auerbach, N. A., and Lewis, B. R.: Biomass and leaf-area index maps derived from SPOT images for Toolik Lake and Imnavait Creek areas, Alaska, Polar Record, 31, 147-154, 1995.

Shutov, V., Gieck, R. E., Hinzman, L. D., and Kane, D. L.: Evaporation from land surface in high latitude areas: a review of methods and study results, Nordic Hydrology, 37, 393-411, doi:10.2166/Nh.2006.022, 2006.

Smith, B., Prentice, I. C., and Sykes, M. T.: Representation of vegetation dynamics in the modelling of terrestrial ecosystems: comparing two contrasting approaches within European climate space, Global Ecol Biogeogr, 10, 621-637, DOI 10.1046/j.1466-822X.2001.t01-1-00256.x, 2001.

Soegaard, H., Hasholt, B., Friborg, T., and Nordstroem, C.: Surface energy- and water balance in a high-arctic environment in NE Greenland, Theor Appl Climatol, 70, 35-51, doi:10.1007/s007040170004, 2001.

Stoy, P. C., Mauder, M., Foken, T., Marcolla, B., Boegh, E., Ibrom, A., Arain, M. A., Arneth, A., Aurela, M., Bernhofer, C., Cescatti, A., Dellwik, E., Duce, P., Gianelle, D., van Gorsel, E., Kiely, G., Knohl, A., Margolis, H., McCaughey, H., Merbold, L., Montagnani, L., Papale, D., Reichstein, M., Saunders, M., Serrano-Ortiz, P., Sottocornola, M., Spano, D., Vaccari, F., and Varlagin, A.: A data-driven analysis of energy balance closure across FLUXNET research sites: The role of landscape scale heterogeneity, Agr Forest Meteorol, 171, 137-152, doi:10.1016/j.agrformet.2012.11.004, 2013.

Sturm, M., Racine, C., and Tape, K.: Climate change. Increasing shrub abundance in the Arctic, Nature, 411, 546-547, doi:10.1038/35079180, 2001.

Stoy, P. C., Williams, M., Spadavecchia, L., Bell, R. A., Prieto-Blanco, A., Evans, J. G., and van Wijk, M. T.: Using Information Theory to Determine Optimum Pixel Size and Shape for Ecological Studies: Aggregating Land Surface Characteristics in Arctic Ecosystems, Ecosystems, 12, 574-589, 10.1007/s10021-009-9243-7, 2009.

Street, L. E., Shaver, G. R., Williams, M., and Van Wijk, M. T.: What is the relationship between changes in canopy leaf area and changes in photosynthetic CO_2 flux in arctic ecosystems?, J Ecol, 95, 139-150, doi:10.1111/j.1365-2745.2006.01187.x, 2007.

Tang, R. L., Li, Z. L., Jia, Y. Y., Li, C. R., Sun, X. M., Kustas, W. P., and Anderson, M. C.: An intercomparison of three remote sensing-based energy balance models using Large Aperture Scintillometer measurements over a wheat-corn production region, Remote Sens Environ, 115, 3187-3202, 10.1016/j.rse.2011.07.004, 2011.

Tanner, C. B., and Jury, W. A.: Estimating evaporation and transpiration from a row crop during incomplete cover, Agron. J., 68, 239–242, 1976.

Timmermans, W. J., Kustas, W. P., Anderson, M. C., and French, A. N.: An intercomparison of the Surface Energy Balance Algorithm for Land (SEBAL) and the Two-Source Energy Balance (TSEB) modeling schemes, Remote Sens Environ, 108, 369-384, doi:10.1016/j.rse.2006.11.028, 2007.

Trochim, E. D., Jorgenson, M. T., Prakash, A., and Kane, D. L.: Geomorphic and biophysical factors affecting water tracks in northern Alaska, Earth and Space Science, 3, 123-141, 10.1002/2015ea000111, 2016.Twine, T. E., Kustas, W. P., Norman, J. M., Cook, D. R., Houser, P. R., Meyers, T. P., Prueger, J. H., Starks, P. J., and Wesely, M. L.: Correcting eddy-covariance flux underestimates over a grassland, Agr Forest Meteorol, 103, 279-300, doi:10.1016/S0168-1923(00)00123-4, 2000.

Vinukollu, R. K., Sheffield, J., Wood, E. F., Bosilovich, M. G., and Mocko, D.: Multimodel Analysis of Energy and Water Fluxes: Intercomparisons between Operational Analyses, a Land Surface Model, and Remote Sensing, J Hydrometeorol, 13, 3-26, 10.1175/2011JHM1372.1, 2012.

Vörösmarty, C. J., Hinzman, L. D., Peterson, B. J., Bromwich, D. H., Hamilton, L. C., Morison, J., Romanovsky, V. E., Sturm, M., and Webb, R. S.: The Hydrologic Cycle and its Role in Arctic and Global Environmental Change: A Rationale and Strategy for Synthesis Study, Fairbanks, Alaska, 84 pp., 2001.

Webb, E. K., Pearman, G. I., and Leuning, R.: Correction of Flux Measurements for Density Effects Due to Heat and Water-Vapor Transfer, Q J Roy Meteor Soc, 106, 85-100, doi:10.1002/qj.49710644707, 1980.

Westermann, S., Luers, J., Langer, M., Piel, K., and Boike, J.: The annual surface energy budget of a high-arctic permafrost site on Svalbard, Norway, Cryosphere, 3, 245-263, 2009.

Wilson, K., Goldstein, A., Falge, E., Aubinet, M., Baldocchi, D., Berbigier, P., Bernhofer, C., Ceulemans, R., Dolman, H., Field, C., Grelle, A., Ibrom, A., Law, B. E., Kowalski, A., Meyers, T., Moncrieff, J., Monson, R., Oechel, W., Tenhunen, J.,

5 Williams, M., Rastetter, E. B., Shaver, G. R., Hobbie, J. E., Carpino, E., and Kwiatkowski, B. L.: Primary production of an arctic watershed: An uncertainty analysis, Ecol Appl, 11, doi:1800-1816, 10.1890/1051-0761, 2001.

Williams, M., Street, L. E., van Wijk, M. T., and Shaver, G. R.: Identifying differences in carbon exchange among arctic ecosystem types, Ecosystems, 9, 288-304, doi:10.1007/s10021-005-0146-y, 2006.

Williamson, S. N., Barrio, I. C., Hik, D. S., and Gamon, J. A.: Phenology and species determine growing-season albedo

10 increase at the altitudinal limit of shrub growth in the sub-Arctic, Glob Chang Biol, 1-11, 10.1111/gcb.13297, 2016.

Wolf, A., Saliendra, N., Akshalov, K., Johnson, D. A., and Laca, E.: Effects of different eddy covariance correction schemes on a energy balance closure and comparisons with the modified Bowen ratio system, Agr Forest Meteorol, 148, 942-952, 10.1016/j.agrformet.2008.01.005, 2008.

Valentini, R., and Verma, S.: Energy balance closure at FLUXNET sites, Agr Forest Meteorol, 113, 223-243, 2002.

15 Xu, L., Myneni, R. B., Chapin, F. S., Callaghan, T. V., Pinzon, J. E., Tucker, C. J., Zhu, Z., Bi, J., Ciais, P., Tommervik, H., Euskirchen, E. S., Forbes, B. C., Piao, S. L., Anderson, B. T., Ganguly, S., Nemani, R. R., Goetz, S. J., Beck, P. S. A., Bunn, A. G., Cao, C., and Stroeve, J. C.: Temperature and vegetation seasonality diminishment over northern lands, Nat Clim Change, 3, 581-586, doi:10.1038/Nclimate1836, 2013.

Yao, J. M., Zhao, L., Gu, L. L., Qiao, Y. P., and Jiao, K. Q.: The surface energy budget in the permafrost region of the

20 Tibetan Plateau, Atmos Res, 102, 394-407, doi:10.1016/j.atmosres.2011.09.001, 2011.

Zhang, K., Kimball, J. S., Nemani, R. R., and Running, S. W.: A continuous satellite-derived global record of land surface evapotranspiration from 1983 to 2006, Water Resour Res, 46, Artn W09522, doi:10.1029/2009wr008800, 2010.

Zhang, Z., Kane, D. L., and Hinzman, L. D.: Development and application of a spatially-distributed Arctic hydrological and thermal process model (ARHYTHM), Hydrol Process, 14, 1017-1044, 2000.

25 Zhuang, Q., Romanovsky, V. E., and McGuire, A. D.: Incorporation of a permafrost model into a large-scale ecosystem model: Evaluation of temporal and spatial scaling issues in simulating soil thermal dynamics, J Geophys Res-Atmos, 106, 33649-33670, doi:10.1029/2001jd900151, 2001.

30
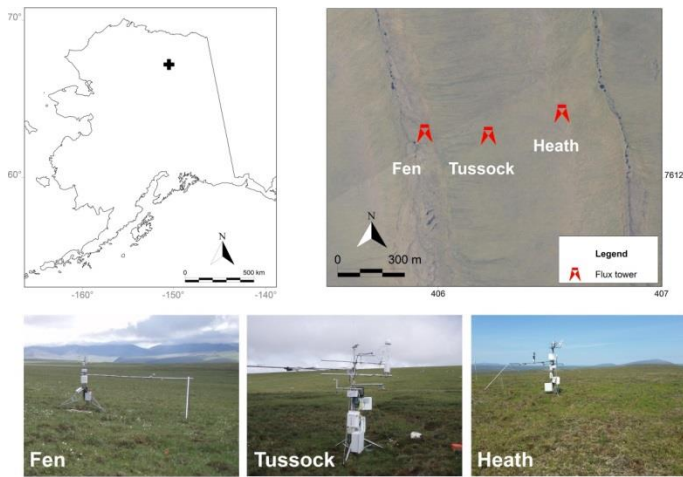
Figure 1: Location of the Fen, Tussock and Heath flux towers at Imnavait watershed. Right panel map is in UTM-6N NAD83 with coordinates in km.
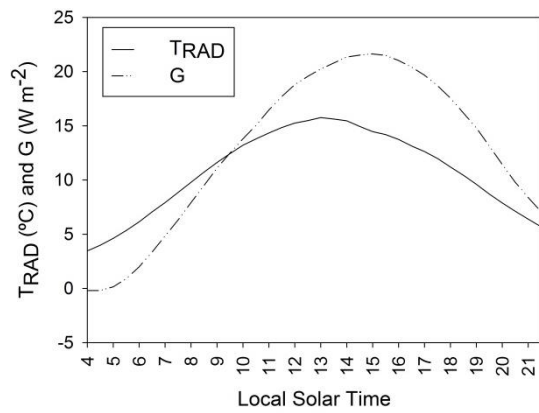
5   **Figure 2. Mean daytime cycle for G and T_{RAD} in the study area computed using all data available from the Fen, Tussock and Heath flux towers from 2008 to 2012.**
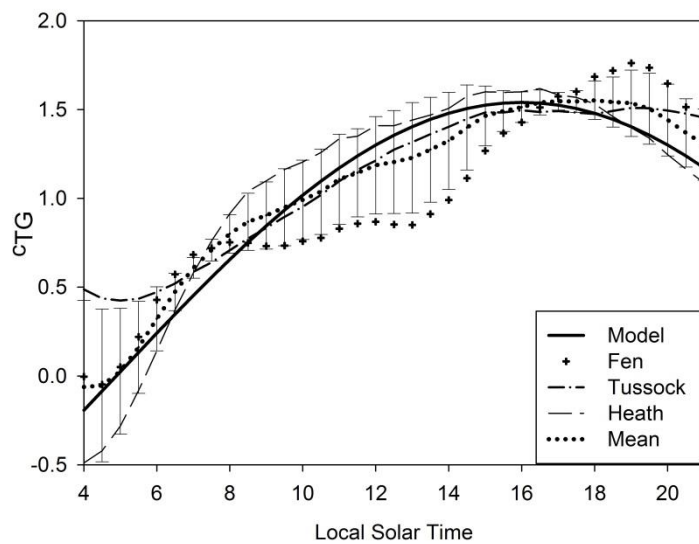
Figure 3. Time series of modelled c_{TG} and observed c_{TG} values from the Fen, Tussock and Heath flux stations as well as mean values for summer conditions (bars represent standard deviation of the mean)

28
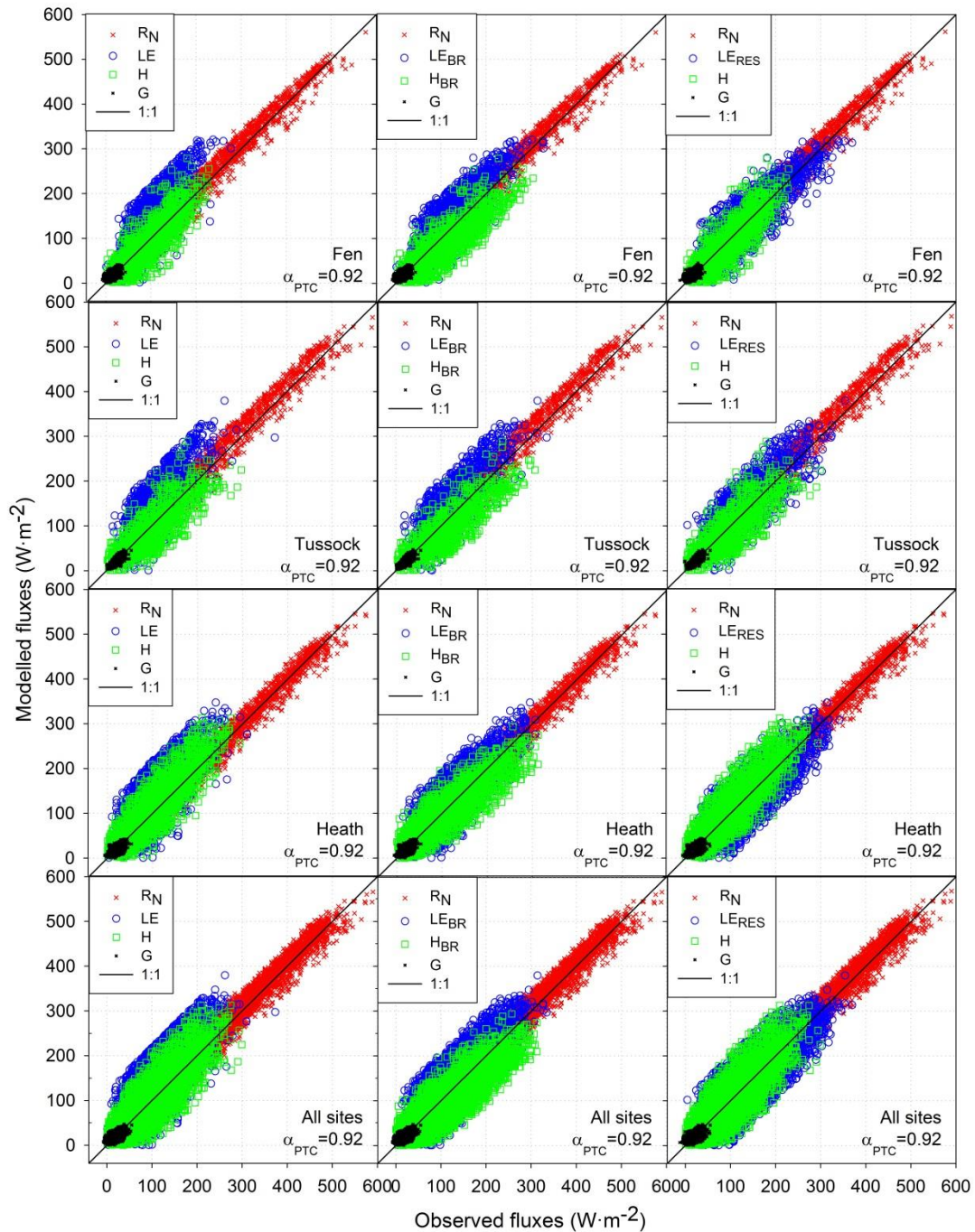
Figure 4. Comparison of modelled vs. measured half-hourly fluxes using α_{PTC} of 0.92. The 1:1 line represents perfect agreement with observations. Columns represent results with unclosed observed turbulent fluxes (left), Bowen ratio closure (middle) and residual closure (right) for the fen, tussock, heath sites and all sites combined (rows).

5
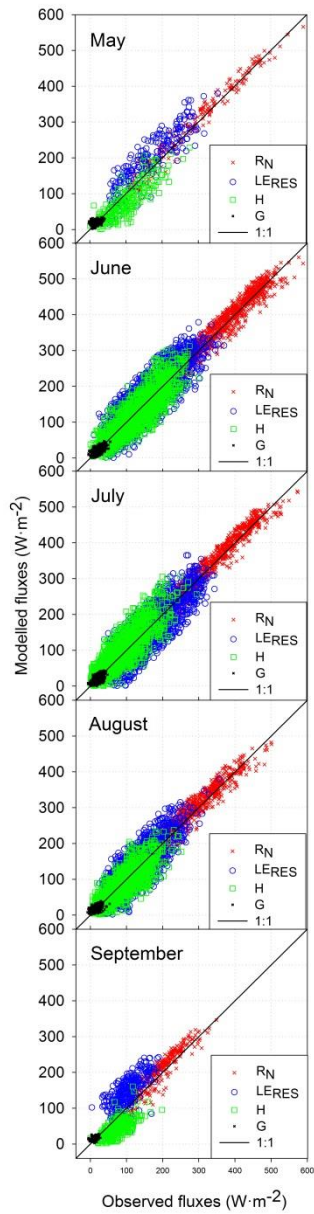
Figure 5. Comparison of modelled vs. observed half-hourly surface fluxes (using LE from residual closure) by month using α_{PTC} of 0.92 and G estimated by the new model. The 1:1 line represents perfect agreement with observations.
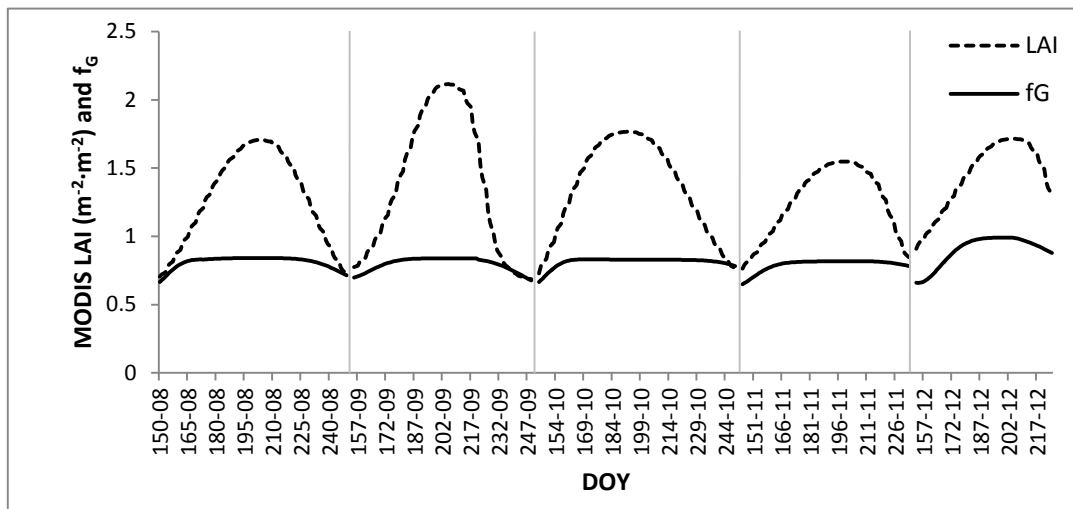
Figure 6. Mean MODIS LAI and fraction of green vegetation (f$_G$) temporal dynamics for all flux stations from 2008 to 2012 .
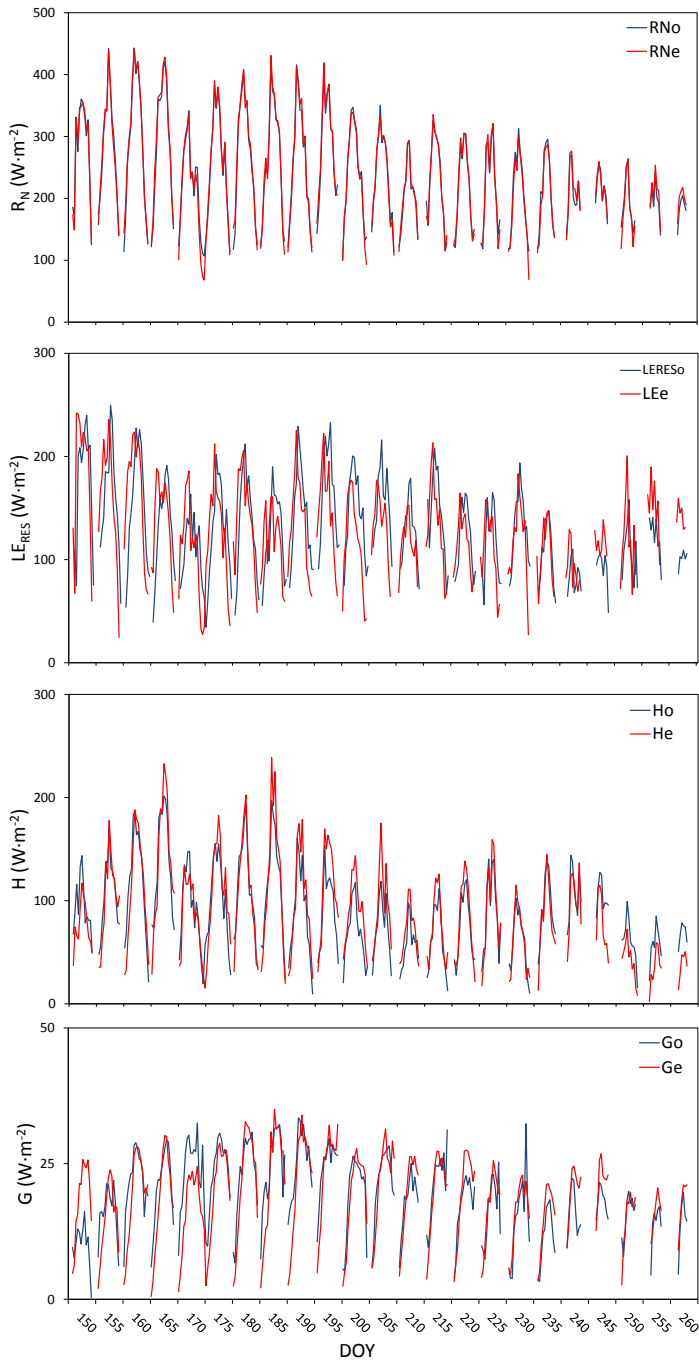
Figure 7. Comparison of hourly flux tower RN, LE, H and G observations (using LE from residual closure) (o) (from 6 to 21 hours local solar time) at the Heath flux tower with model estimates (e) using αPTC of 0.92. Each diurnal segment represents flux data averaged by hour over 5-day intervals from 2008 to 2012.
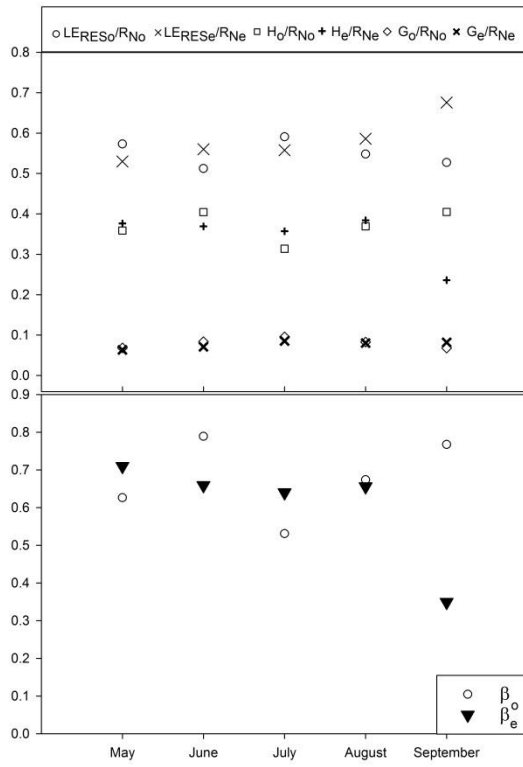
Figure 8. Monthly mean observed (o) and estimated (e) energy partitioning (LE/RN, H/RN and G/RN) and Bowen ratio (β) for all flux stations from 2008 to 2012 using αPTC of 0.92.

5

10

15

Flux station name			Fen	Tussock	Heath
Coordinates (lat, long - WGS84)			68.606, -149.311	68.606, -149.304	68.607, -149.296
Period (Year|Day of Year)			2008|194-252	2009|194-253	2008|194-252
			2010|142-262	2010|142-262	2009|159-253
			2011|217-262	2012|156-226	2010|143-262
			2012|153-264		2011|147-262
					2012|156-226
TSEB inputs	**Symbol**	**Units**			
Wind speed	u	m s^{-1}	3.3 ± 1.7	3.4 ± 1.4	3.4 ± 1.4
Air temperature	T_a	°C	11.6 ± 3.5	12.8 ± 3.8	12.8 ± 3.8
Vapor pressure	e_a	kPa	0.9 ± 0.2	1 ± 0.3	1 ± 0.3
Atmospheric pressure	P	kPa	92 ± 0.2	90 ± 0.6	90 ± 0.6
Solar radiation	S_d	W·m^{-2}	432 ± 121	503 ± 149	503 ± 149
Longwave incoming radiation	L_d	W·m^{-2}	261 ± 37	245 ± 34	245 ± 34
Surface temperature	T_s	K	288 ± 4	290 ± 5	290 ± 6
Leaf area index (MODIS)	LAI	m^2·m^{-2}	1.15 ± 0.32	1.28 ± 0.42	1.25 ± 0.4
Canopy height	h_c	m	0.4	0.4	0.4
Clumping factor	Ω_c		1	1	1
Fraction of green vegetation	f_g		0.92 ± 0.01	0.9 ± 0.03	0.9 ± 0.03

Table 1. Flux station name and location, period of model evaluation and list of inputs required by the TSEB. Average and standard deviation for the input values were computed for the full period of model evaluation for each site.

Instrument	Description	Height/*Depth*(m)
Campbell Sci. CSAT3	Three Dimensional Sonic Anemometer	2.18 - 3.18
Licor LI-7500	Open Path Infrared Gas Analyzer (CO_2 and H_2O)	2.18 - 3.18
Vaisalla HMP45C	Temperature and Relative Humidity Probe	1.93 - 2.82
Hukseflux HFP01SC	Self-calibrating Soil Heat Flux Plates (four per site)	*0.08*
Campbell Sci. TCAV	Type E Thermocouple Averaging Soil Temperature Probes (two per site)	*0.02-0.04*
Campbell Sci. CS616	Water Content Reflectometers (two per site)	*0.025*
Licor LI190SB	PAR Sensor (incoming)	2 - 3.6
Licor LI190SB	PAR Sensor (outgoing)	2

Met One Ins. 014A	Wind Speed Sensor	1.5 - 2.26
Kipp & Zonen CMA6	Pyranometer/Albedometer	2
*Kipp & Zonen CNR4	Four components net Radiometer	2
Kipp & Zonen NR-Lite	Net radiation	2
Apogee IRR-P	InfraRed Radiometer Sensor	1.5 - 3

Table 2. General overview of the Fen, Tussock and Heath flux sites instrumentation (more information available at: http://aon.iab.uaf.edu/imnavait). Apogee infrared radiometers were oriented 45º off-nadir at the three flux stations. Asterisk (*) means that this instrument is only available at the Tussock flux station.

			SF03					K98				
	c_G	n	R^2	RMSE	MBE	MAD	MADP	R^2	RMSE	MBE	MAD	MADP
Fen	0.30	1558	0.04	23	3	20	128	0.01	40	23	31	199
	0.14		0.04	15	-7	12	76	0.01	15	2	11	73
Tussock	0.30	1273	0.18	23	3	18	78	0.05	39	21	32	138
	0.14		0.23	17	-11	12	53	0.05	15	-4	11	46
Heath	0.30	2347	0.11	26	-5	20	96	0.10	34	14	26	125
	0.14		0.14	21	-14	15	72	0.06	16	-5	10	48
Total	0.30	5178	0.12	25	0	20	98	0.03	37	19	29	145
	0.14		0.10	18	-11	14	68	0.03	15	-3	11	53

Table 3. Performance statistics for the soil heat flux estimation using Santanello and Friedl (2003), SF03, and Kustas et al. (1998), K98, methodologies and two values for the maximum c_G value. RMSE, MBE and MAD are in W·m^{-2} and MADP in %.

	Fit subset (60%)				Test subset (40%)				Flux dataset			
	Fen	Tussock	Heath	Total	Fen	Tussock	Heath	Total	Fen	Tussock	Heath	Total
R^2	0.89	0.99	0.99	0.99	0.55	0.77	0.69	0.68	0.27	0.56	0.49	0.44
RMSE	3.9	1	1	1	7	5	6	6	9	5	7	7
MBE	1.7	-0.2	-0.6	0.1	0.6	-0.3	-0.3	0	3.9	0.5	-0.3	1
MAD	2.8	1	1	1	5	4	5	4	7	4	5	6
MAPD	25	8	8	8	49	28	38	37	44	17	24	28
n	8283	10332	10748	29363	3310	4122	4273	11705	1558	1273	2347	5178

Table 4. Accuracy statistic for the new c_{TG} approach for the fit and the test. RMSE, MBE and MAD in W·m^{-2}, MADP in % and n is number of half-hour intervals.

R_N	n	R^2	RMSE	MBE	MAD	MAPD
Fen	1558	0.99	23	8	18	7
Tussock	1273	0.99	25	12	19	7
Heath	2347	0.99	20	2	15	6
Total	5178	0.99	23	7	18	7

LE	n	R^2	RMSE	MBE	MAD	MAPD
Fen	1558	0.54	47	27	37	36
Tussock	1273	0.52	61	44	51	41
Heath	2347	0.55	54	33	44	42
Total	5178	0.54	53	35	44	40

LE_{BR}	n	R^2	RMSE	MBE	MAD	MAPD
Fen	1558	0.76	45	25	37	30
Tussock	1273	0.66	52	33	43	33
Heath	2347	0.65	43	15	35	28
Total	5178	0.71	46	23	38	35

LE_{RES}	n	R^2	RMSE	MBE	MAD	MAPD
Fen	1558	0.74	37	9	29	21
Tussock	1273	0.68	45	24	38	26
Heath	2347	0.68	39	-3	31	21
Total	5178	0.69	40	7	32	30

H	n	R^2	RMSE	MBE	MAD	MAPD
Fen	1558	0.66	28	-6	22	23
Tussock	1273	0.65	33	-12	26	24
Heath	2347	0.71	33	4	26	26
Total	5178	0.67	32	-3	25	25

H_{BR}	n	R^2	RMSE	MBE	MAD	MAPD
Fen	1558	0.69	39	-24	31	27
Tussock	1273	0.67	39	-22	29	26
Heath	2347	0.72	38	-14	30	25
Total	5178	0.69	39	-19	31	30

Table 5. Accuracy and error statistics from the comparison of modelled vs. observed unclosed and closed surface fluxes surface fluxes using α_{PTC} of 0.92. n is the number of half-hour periods analysed. RMSE, MAD and MBE are in W·m^{-2} and MADP in %.

5

10

15

		R_N								LE				
	n	R^2	RMSE	MBE	MAD	MAPD		n	R^2	RMSE	MBE	MAD	MAPD
Fen	1558	0.99	23	8	18	7	Fen	1558	0.66	58	45	52	45
Tussock	1273	0.99	25	12	19	7	Tussock	1273	0.54	59	52	50	48
Heath	2347	0.99	20	2	15	6	Heath	2347	0.52	57	39	47	42
Total	5178	0.99	23	7	18	7	Total	5178	0.59	58	45	50	45

		LE_{BR}								LE_{RES}				
	n	R^2	RMSE	MBE	MAD	MAPD		n	R^2	RMSE	MBE	MAD	MAPD
Fen	1558	0.73	52	36	43	35	Fen	1558	0.76	41	20	34	24
Tussock	1273	0.64	56	40	48	37	Tussock	1273	0.7	53	36	45	31
Heath	2347	0.66	48	26	40	32	Heath	2347	0.71	40	9	32	22
Total	5178	0.66	51	32	43	40	Total	5178	0.7	44	19	36	33

		H								H_{BR}				
	n	R^2	RMSE	MBE	MAD	MAPD		n	R^2	RMSE	MBE	MAD	MAPD
Fen	1558	0.62	33	-18	26	27	Fen	1558	0.64	46	-34	38	33
Tussock	1273	0.6	39	-24	31	29	Tussock	1273	0.62	43	-29	35	28
Heath	2347	0.67	33	-8	26	26	Heath	2347	0.65	43	-25	35	28
Total	5178	0.64	35	-15	28	27	Total	5178	0.64	44	-29	36	36

Table 6. Accuracy and error statistics from the comparison of modelled vs. observed unclosed and closed surface fluxes using α_{PTC} of 1.26. n is the number of half-hour periods analysed. RMSE, MAD and MBE are in W·m^{-2} and MADP in %.

		R_N					LE				
	n	R^2	RMSE	MBE	MAD	MAPD	R^2	RMSE	MBE	MAD	MAPD
May	227	0.99	24	7	19	7	0.78	46	28	38	23
June	1727	0.99	22	6	17	6	0.73	40	11	32	20
July	1647	0.99	21	5	17	6	0.72	39	-7	31	20
August	1264	0.99	23	6	19	8	0.64	37	7	30	24
September	312	0.99	26	14	23	12	0.44	52	39	46	45

		H					G				
	n	R^2	RMSE	MBE	MAD	MAPD	R^2	RMSE	MBE	MAD	MAPD
May	227	0.69	36	-22	29	27	0.12	10	1	8	48
June	1727	0.71	32	-6	25	20	0.45	7	0	6	26
July	1647	0.72	32	10	25	29	0.49	6	1	5	23
August	1264	0.62	37	7	30	24	0.40	7	3	6	34

| September | 312 | 0.39 | 38 | -31 | 32 | 42 | 0.27 | 7 | 4 | 5 | 40 |

Table 7. Mean monthly accuracy and error statistics from the comparison of modelled vs. observed surface fluxes (using LE from residual closure) using αPTC of 0.92. n is the number of half-hour periods analysed. RMSE, MAD and MBE are in W·m⁻² and MADP in %.

5